EUROPEAN RESPIRATORY *journal*

FLAGSHIP SCIENTIFIC JOURNAL OF ERS

Early View

Original research article

Eosinophils Protect Against Pulmonary Hypertension through 14-HDHA and 17-HDHA

Ting Shu, Jiawei Zhang, Yitian Zhou, Zhihua Chen, Jinqiu Li, Qihao Tang, Wenqi Lei, Yanjiang Xing, Jing Wang, Chen Wang

Please cite this article as: Shu T, Zhang J, Zhou Y, *et al*. Eosinophils Protect Against Pulmonary Hypertension through 14-HDHA and 17-HDHA. *Eur Respir J* 2022; in press (https://doi.org/10.1183/13993003.00582-2022).

Eosinophils Protect Against Pulmonary Hypertension through 14-HDHA and 17-HDHA

Ting Shu, MD, PhD[1,†], Jiawei Zhang, PhD[1,†], Yitian Zhou, MD[1, 2], Zhihua Chen, PhD[3], Jinqiu Li, PhD[4], Qihao Tang, PhD[1], Wenqi Lei, PhD[1], Yanjiang Xing, PhD[4,*], Jing Wang, MD, PhD[1,*], Chen Wang, MD, PhD[1,4]

[1] State Key Laboratory of Medical Molecular Biology, Haihe Laboratory of Cell Ecosystem, Department of Pathophysiology, Institute of Basic Medical Sciences, Chinese Academy of Medical Sciences and Peking Union Medical College, Beijing, China.

[2] Peking Union Medical College, MD Program, Beijing, China.

[3] Key Laboratory of Respiratory Disease of Zhejiang Province, Department of Respiratory and Critical Care Medicine, Second Affiliated Hospital of Zhejiang University School of Medicine, Hangzhou, Zhejiang, China.

[4] State Key Laboratory of Medical Molecular Biology, Department of Physiology, Institute of Basic Medical Sciences, Chinese Academy of Medical Sciences, Peking Union Medical College, Beijing, China.

Short title: Eosinophils Alleviate Pulmonary Hypertension

*Corresponding author:

Dr. Jing Wang, State Key Laboratory of Medical Molecular Biology, Haihe Laboratory of Cell Ecosystem, Department of Pathophysiology, Institute of Basic Medical Sciences, Chinese Academy of Medical Sciences and Peking Union Medical College, Beijing, China. E-mail: wangjing@ibms.pumc.edu.cn, Phone: 86-10-69156477

Dr. Yanjiang Xing, State Key Laboratory of Medical Molecular Biology, Haihe Laboratory of Cell Ecosystem, Department of Physiology, Institute of Basic Medical Sciences, Chinese Academy of Medical Sciences, Peking Union Medical College, Beijing, China. E-mail: xingyanjiang@ibms.pumc.edu.cn, Phone: 86-10-65105092

† These authors contributed equally to this manuscript.

Total word count: 4905

Abstract

Background: Pulmonary hypertension (PH) is a life-threatening disease featured by pulmonary vessel remodelling and perivascular inflammation. Whether and how eosinophils (EOS) affect PH development remain unclear.

Methods: EOS infiltration and chemotaxis were investigated in peripheral blood and lung tissues from pulmonary arterial hypertension (PAH) patients without allergic history and sugen/hypoxia-induced PH mice. *GATA1*-deletion (ΔdblGATA) mice, anti-IL5 antibody-treated mice and rats were applied to investigate the role of EOS deficiency in PH development. UHPLC-MS/MS was conducted to identify the critical oxylipin molecule(s) produced by EOS. The culture supernatants and lysates of EOS were collected to explore the mechanisms in co-culture cell experiments.

Results: EOS percentage was lower in peripheral blood while infiltration was higher in lung tissues from PAH patients and PH mice. PAH/PH lungs showed increased EOS-related chemokine expression, and CCL11 derived from adventitial fibroblasts potentially mediated EOS migration into lungs. EOS deficiency aggravated sugen/hypoxia-induced PH and pulmonary vascular muscularization in mice and rats, accompanied by increased neutrophil and monocyte/macrophage infiltration. In addition, EOS prevented PDGFbb-induced pulmonary arterial smooth muscle cell (PASMC) proliferation and migration *in vitro*. EOS highly expressed arachidonate 15-lipoxygenase (ALOX15), and EOS deficiency largely repressed ALOX15 expression in lungs. UHPLC-MS/MS revealed 14-hydroxy docosahexaenoic acid (14-HDHA) and 17-HDHA as downstream oxylipins produced by EOS. 14/17-HDHA showed anti-inflammatory effects on recruitment of neutrophils and monocytes/macrophages through formyl peptide receptor 2, and they repressed proliferation by activating peroxisome proliferator-activated receptor γ and blunting Stat3 phosphorylation in PASMCs.

Conclusions: In PH development without external inflammatory stimulus, peripheral blood exhibits a low EOS level, in which EOS play a protective role through suppressing perivascular inflammation and maintaining PASMC homeostasis via 14/17-HDHA.

Keywords: eosinophil, pulmonary hypertension, vascular remodelling, eicosanoids

Non-standard Abbreviations and Acronyms

PH, pulmonary hypertension

PAH, pulmonary arterial hypertension

EOS, eosinophil

SuHx, sugen/hypoxia

scRNA-seq, single-cell RNA sequencing

WT, wild type

KO, knockout

ΔdblGATA, GATA1 deletion

RVSP, right ventricular systolic pressure

RV/LV+S, ratio of the weight of right ventricle to the weight of left ventricle plus septum

α-SMA, α-smooth muscle actin

CCL11, C-C motif chemokine 11 (Eotaxin-1)

CCL24, C-C motif chemokine 24 (Eotaxin-2)

CCL26, C-C motif chemokine 26 (Eotaxin-3)

IL5, interleukin 5

COX, cyclooxygenase

LOX, lipoxygenase

TGFβ, transforming growth factor β

BMPR2, bone morphogenetic protein receptor 2

PDGF, platelet-derived growth factor

ALOX15, arachidonate 15-Lipoxygenase

14-HDHA, 14-hydroxy docosahexaenoic acid

17-HDHA, 17-hydroxy docosahexaenoic acid

FPR2, formyl peptide receptor 2

PPARγ, peroxisome proliferators-activated receptor γ

Introduction

Pulmonary arterial hypertension (PAH) is a severe life-threatening disease, featured by pulmonary vascular remodelling and perivascular inflammatory cell infiltration[1]. An enhanced Th2 immune response in PAH has been reported for years[2, 3]. However, the role of eosinophils (EOS), one of the Th2 effector cells[4], in PAH is seldom reported. A previous study showed that PAH patients with worse syndromes had lower circulating EOS levels[5]; however, the functions of EOS in regulation of PAH development and the detailed mechanisms remain unclear.

EOS are granulocytes with segmented nuclei and eosinophilic granules[6], which mature in bone marrow under a tightly regulated process directed by various transcription factors such as GATA1, GATA2 and FOG1, and cytokines such as IL5, and then are released into peripheral blood[7, 8]. Chemokines such as CCL11 (eotaxin-1), CCL24 (eotaxin-2), and CCL26 (eotaxin-3) and cytokines such as IL5 promote EOS to transmigrate into tissues[8, 9]. Once they have trafficked into tissues, EOS function in the following processes: a) degranulation and cytokine release[10, 11]; b) DNA release and eosinophil extracellular traps (EETs) formation[12-14]; and c) lipid metabolite production[6, 15, 16]. These processes facilitate interaction of EOS with immune cells[15, 16] or tissue resident cells[10, 11]. The detrimental roles of EOS have been widely recognized for decades, especially in asthma[4, 12]: EOS interact with mast cells[17], aid B cells to produce antibodies[18, 19], promote Th2 polarization[20], and mediate epithelial damage[4, 21]. However, EOS have regained attention in recent years because they show protective effects in maintaining tissue homeostasis in heart[11], lung[15], liver[22], gut[16], and adipose tissue[23, 24], which suggests that EOS have distinct roles in physiology and pathophysiology processes.

To determine whether and how EOS affect PAH development, we explored the function and underlying mechanisms of lung EOS in PAH patients and sugen/hypoxia (SuHx)-induced PH rat or mouse model. We found that EOS migrated from peripheral blood to lung tissues in PAH patients and PH mice. By using ΔdblGATA mice and anti-IL5 antibody (TRFK5) -treated mice and rats, we found EOS deficiency worsened PH development by aggravating perivascular inflammation and pulmonary arterial smooth muscle cell (PASMC) proliferation in animal models. Finally, we showed that EOS functioned by releasing lipid mediators, among which 14-hydroxy

docosahexaenoic acid (14-HDHA) and 17-HDHA exerted protective effect in PH.

Methods

Human subjects

From 2016 to 2018, we enrolled 123 patients with either idiopathic or heritable PAH (IPAH or HPAH) and 119 healthy controls that were sex- and age-matched into our single-center clinical study in Fuwai Hospital. Patients with IPAH/HPAH had been diagnosed using the 2015 ESC/ERS guidelines[25], and these diagnoses were also compatible with the IPAH/HPAH criteria described in the 6th World Symposium on Pulmonary Hypertension, 2018[26]. We excluded patients that were found to have (i) allergy, infection, or autoimmune diseases; (ii) tumors or fibrosis; or (iii) an age younger than 18. Potential subjects were screened with a patient health questionnaire to establish their medical history. In the healthy control group, subjects with no history of PH, cardiovascular diseases, pulmonary diseases, cancer, infection, allergy, or autoimmune diseases were included, and patients with an abnormal BMI or aberrant routine blood work results were excluded. Lung tissue samples from five PAH patients were obtained through the China-Japan Friendship Hospital Lung Transplantation Center between 2018 and 2019. Lung tissue specimens found to have (i) a lung infection, (ii) allergic diseases or autoimmune diseases, or (iii) complicated pulmonary diseases (such as tumors, fibrotic regions, etc.) were excluded. For our control group, five non-PAH lung tissue samples originating from healthy transplant donors were collected. Enrolled subjects gave informed consent to participate in this study. Approval for this study was provided by the Institutional Ethics Committee of Peking Union Medical College (2018043) and Fuwai Hospital (Approval NO. 2017-877).

Animal models

ΔdblGATA mice were purchased from the Jackson Laboratory (033551, Bar Harbor, ME). Male hemizygote mice (ΔdblGATA/Y) and female heterozygote mice (ΔdblGATA/+) were maintained in a C57BL/6 genetic background to generate WT(+/Y) and KO littermates (ΔdblGATA/Y). C57BL/6 mice and Sprague Dawley rats were purchased from Beijing Vital River Laboratory Animal Technology Co., Ltd. Animals were randomly assigned to various treatment groups for each experiment. Mice or rats were maintained on a 12-h-light-dark cycle with a regular unrestricted diet. To establish a SuHx-induced PH mouse model, 8-10-week-old male or female

mice received weekly subcutaneous injections of SU5416 (20 mg/kg, S8442, Sigma Aldrich) for 3 weeks and were housed in an airtight plexiglass chamber (China Innovation Instrument) with 10% O_2[27]. To establish a SuHx-induced PH rat model, 200 g male rats received a single SU5416 injection (20 mg/kg) and were then housed in 10% O_2 for three weeks. For the EOS depletion mice model, the anti-IL5 neutralizing antibody TRFK5 (554391, BD Pharmingen) was administrated at a dose of 2 μg/mouse each week, with a total of three doses for each mouse, through intravenous injection[28]. Sex- and age-matched littermates injected with an equal dose of isotype control antibody (IgG1κ, 559072, BD Pharmingen) were used as controls. For the EOS depletion rat model, anti-IL5 neutralizing antibody TRFK5 (14-7052-85, Invitrogen) was administrated at a dose of 17.5 μg/rat each week, three doses for each rat, and isotype control antibody was injected at an equal volume. For FPR2 agonist Ac2-26 (HY-P1098A, MCE) injection, mice were intraperitoneally injected at a dose of 50 μg/mouse every three days. The control mice were injected with an equal volume of vehicle. All animal experiments were conducted under the approval of the Animal Research Committee of the Institute of Laboratory Animals, Chinese Academy of Medical Sciences, and Peking Union Medical College (ACUC-A01-2020-017).

Additional materials and methods are available in the supplementary material.

Results

EOS populations decrease in blood while lung infiltration increases in PAH patients

To examine changes in EOS abundance during PAH progression, we enrolled 123 IPAH/HPAH patients and 119 age-/sex-matched healthy control subjects (Supplementary Table 1). Quantification of EOS by routine tests in peripheral blood samples indicated that the EOS percentage in PAH patients was significantly lower than that in sex-matched healthy control subjects (Figure 1A). Further classification of PAH patients according to the New York Heart Association (NYHA) revealed that type I/II patients had a higher proportion of EOS in peripheral blood compared with type III/IV patients (Figure 1B). These observations were both consistent with

previous reports[5]. Notably, loss-of-function mutations of bone morphogenetic protein receptor 2 (*BMPR2*) are found in IPAH/HPAH, and patients who carry a causative mutation in *BMPR2* show more severe vascular dysfunction[29]. Here, we found that carriers of *BMPR2* mutation also had a lower percentage of EOS in peripheral blood than non-carriers (Figure 1C). To further examine changes in the abundance of EOS in lung tissues associated with PAH, we conducted EOS staining assays of lung tissue samples from PAH and non-PAH subjects. Hematoxylin and eosin (H&E) staining indicated enhanced EOS infiltration into PAH lung tissues, characterized by the accumulation of red-staining granulocytes with segmented nuclei around remodelled pulmonary vessels (Figure 1D). Immunohistochemistry staining showed that ECP^+ EOS were more abundant in PAH lungs than in non-PAH lungs (Figure 1D and E). By immunofluorescence staining, we found that most ECP^+ EOS were located closer to $Vimentin^+$ adventitial layer (Figure 1F, arrow a), and ECP^+ EOS adhering to $CD31^+$ endothelial cells in vascular lumen were also spotted (Figure 1F, arrow b). These observations suggest a dynamic process of EOS migration, recruited from peripheral blood and resided in parenchyma. Further supporting the observed increase in EOS pulmonary migration, the expression of *IL5* and Eotaxin genes (*CCL11*, *CCL24*, and *CCL26*), which are necessary for EOS trafficking, was significantly elevated in PAH lung tissues (Figure 1G), suggesting enhanced EOS recruitment in lungs during PAH development.

Taken together, these results indicate that EOS migrate to lung tissue during the progression of PAH in humans.

Decreased percentage of EOS in blood and increased proportions of EOS in lungs of PH mice

To determine whether these changes in EOS during PAH could also be observed in mice, we next established a SuHx-induced PH mouse model. We conducted flow cytometry analysis by staining for $CD45^+CD11b^+SiglecF^+$ EOS and found that the percentage of EOS in blood was significantly lower in PH mice compared with that in control mice (Figure 2A), while the percentage of EOS in PH lung tissue was significantly higher (Figure 2B). EOS infiltration into lungs was then confirmed by H&E and SiglecF staining (Figure 2C). In addition, analyses of cytokine and

chemokine expression indicated that both mRNA and protein expression of these markers were elevated in lung tissues of PH mice compared with controls (Figure 2D and E). These findings were in agreement with our above results from PAH patients.

No significant changes were observed in EOS levels in either bone marrow or spleen (Figure 2F and G), suggesting that the production of EOS was unaffected during PH progression. However, EOS quantification showed a slight but significant increase in the percentage of EOS in remodelled right ventricle tissues (Figure 2H), but no difference from controls in the left ventricle (Figure 2I), suggesting that EOS may be related to impaired right ventricle function in PH. In lung tissues, EOS are classified as either resident eosinophils (rEOS) or inflammatory eosinophils (iEOS) based on CD101 expression[20]. Here we found that although there was slight decrease in the percentage of $CD101^-$ rEOS (from 91.2% to 85.4%) in PH lungs compared with controls (Supplementary Figure 1A), they were still the predominant subtype in lung and peripheral blood under PH (Supplementary Figure 1A and B) and the only detectable subtype in bone marrow of mice (Supplementary Figure 1C).

Collectively, these results show that the proportion of EOS decreases in blood but increases in lungs of PH mice, similar to what was observed in PAH patients.

CCL11 upregulation in adventitial fibroblasts of PH lungs is associated with EOS recruitment

In light of our observations of pulmonary EOS migration during PH, we next examined EOS trafficking-related cytokine and chemokine expression. Among all genes tested, *CCL11* (*Eotaxin-1*) was the most highly expressed in mouse lungs (Supplementary Figure 2). Subsequent single-cell RNA sequencing (scRNA-seq) analysis of lung tissues from healthy humans (Figure 3A) and control mice (Figure 3B) revealed that a considerable proportion of fibroblasts expressed high levels of *CCL11* in both species. Further comparison of fibroblasts from PH mice showed that *Ccl11* was primarily expressed in adventitial rather than alveolar fibroblasts, and that both the percentage of cells and the average expression levels were greater in PH lung tissues than in control (Figure 3C). Immunostaining of lung tissue from PAH patients and SuHx-induced PH mice showed that the area of tissue expressing CCL11 overlapped with that expressing the platelet-derived growth factor receptor alpha

(PDGFRa), which confirmed that CCL11 was derived from fibroblasts (Figure 3D and E). However, CCL11 did not co-localize with CD31, a-SMA, CD45, or CC10, which further suggested that neither endothelial cells, smooth muscle cells, immune cells, nor epithelial cells were the main source of CCL11 in lungs of PH mice (Supplementary Figure 3A-D). In human and mouse pulmonary adventitial fibroblasts (PAFs) activated with transforming growth factor β (TGFβ) or PDGFbb, we found that *CCL11* expression was significantly higher than that in untreated cells (Figure 3F and G). Moreover, *CCL11* was not obviously upregulated in similarly treated endothelial cells or smooth muscle cells (Supplementary Figure 3E and F), allowing us to exclude these cell types as the main source of CCL11 during PH development. Using EOS adhesion assay, we found that CCL11 stimulation increased EOS adhesion to endothelial cells (Figure 3H), supporting the chemotaxis role of CCL11 for EOS recruitment. Collectively, these results suggest that impaired function of PAFs during PAH development result in enhanced CCL11 expression, which in turn promotes EOS migration.

EOS deficiency aggravates PH in animal models

To better understand the functional role of EOS in PH development, we induced PH in male EOS-deficient ΔdblGATA mice by exposing them to SuHx (Supplementary Figure 4, Figure 4A). We first confirmed that the ΔdblGATA mice were deficient in EOS compared with wild-type (WT) mice (Figure 4B, quantified in 4C). In addition, ΔdblGATA mice exhibited a significantly higher right ventricular systolic pressure (RVSP) and RV hypertrophy index (RV/LV+S) compared with WT under PH (Figure 4D and E), indicating that the deficiency of EOS further aggravated PH development. Immunostaining also showed that vascular thickening (Figure 4F, quantified in G) and muscularization (Figure 4H) were more extensive in the absence of EOS in PH. Although fibroblasts were implicated in EOS recruitment (Figure 3), no significant changes in pulmonary fibrosis were observed in EOS-deficient PH mouse lungs (Supplementary Figure 5A and B).

Since IL5 is crucial for EOS maturation and migration[8], depletion of EOS through IL5 neutralization is applied clinically as a treatment for asthma[30]. Therefore, we depleted EOS by neutralizing IL5 in C57BL/6 male mice. After injection with

anti-IL5 antibody (TRFK5), we induced PH in both TRFK5 treated male mice and isotype control treated male mice (Figure 4I). We found that the percentage of EOS was significantly lower in lung tissues of mice treated with TRFK5, compared with that in isotype control treated mice (Figure 4J and K). Furthermore, TRFK5 treatment resulted in a higher RVSP and RV/LV+S in PH mice (Figure 4L and M). Consistent with these observations, we also noted that vascular muscularization was more extensive in EOS-depleted PH mice (Figure 4N-P), without affecting pulmonary fibrosis (Supplementary Figure 5C and D). As PAH onset are more predominant in females, we also examined the role of EOS in female mice by TRFK5 injection (Supplementary Figure 6A). Consistent with the observations in male mice, more severe pulmonary hypertension phenotypes were observed in female PH mice with EOS depletion compared to isotype control treated mice (Supplementary Figure 6B-G).

As the rat PH model exhibited more severe progress than mouse PH model, and shared more similarity with human PAH, we further explored the role of EOS in the SuHx-induced rat PH model. Male rats that received TRFK5 treatment showed decreased blood EOS percentage (Supplementary Figure 7A and B). In SuHx-induced rat PH model, EOS depletion exhibited more severe PH development and vascular muscularization, which is consistent with the observations in mouse model (Supplementary Figure 7C-G).

Taken together, these results show that genetically or chemically induced EOS deficiency aggravates PH development, suggesting that EOS have a protective effect in PH development.

EOS deficiency leads to increased neutrophil and monocyte/macrophage infiltration during PH

We next sought to precisely define the effects of EOS in PH development. Since previous studies have shown that EOS participate in regulating immune homeostasis processes, such as Th2 polarization[20], mast cell infiltration[17], and B cell immunoglobulin production[18, 19], we examined how EOS deficiency affects different immune cell populations during PH in mice. Using flow cytometry-based assays to quantify infiltration of different immune cells in ΔdblGATA mice, we

observed no significant changes in the percentages of B cells, T cells (Th cells and CTL cells), mast cells, or dendritic cells compared with those in WT mice (Supplementary Figure 8A-E) under PH. ELISA-based detection of immunoglobulin subtype levels indicated that EOS deficiency did not affect IgE, IgG, or IgA production in lung tissues of PH mice (Supplementary Figure 8F-H).

Interestingly, we found increased proportions of $CD45^+CD11b^+Ly6G^+$ neutrophils and $CD45^+CD11b^+Ly6C^+$ monocytes/macrophages in lung tissues of EOS-deficient PH mice (Figure 5A and B). Immunofluorescent staining further showed more $Ly6G^+$ neutrophils and $CD68^+$ monocytes/macrophages located around remodelled pulmonary vessels in lung tissues of EOS-deficient ΔdblGATA mice under PH (Figure 5C and D). EOS depletion in TRFK5-treated mice also led to increased infiltration of neutrophils and monocytes/macrophages into lung tissues compared with that in the isotype control mice with induced PH (Figure 5E-H, Supplementary Figure 6H and I), without affecting other immune cell types (Supplementary Figure 9).

These observations of enhanced neutrophil and monocyte/macrophage infiltration indicate that EOS deficiency or depletion aggravates the PH-related inflammation of lung tissue in mice.

EOS suppress PASMC proliferation and migration

Increased pulmonary vascular muscularization in ΔdblGATA mice during PH suggests a role for EOS in sustaining smooth muscle cells. To test this hypothesis, bone marrow-derived EOS were cultured, and the lysates and supernatants of harvested cells were used to treat PASMCs (Figure 6A). After 14 days of culture, the percentage of $CD45^+CD11b^+SiglecF^+$ EOS in the total cell population reached 95% (Figure 6B). PDGFbb-induced PASMC proliferation and migration were effectively suppressed by EOS lysates (Figure 6C and D, quantified in G) and culture supernatants (Figure 6E and F, quantified in H) in a dose-dependent manner. These observations suggest a beneficial role of EOS in regulating PASMC function.

14/17-HDHA contribute to the protective role of EOS in PH mice

Having revealed that EOS have anti-inflammatory and anti-proliferative effects in PH mice, we next sought to identify the essential underlying mechanism. One potential mechanism is the degranulation of EOS; however, we excluded this as a possibility, as it seldom happens in mice[31]. Another mechanism is EETs formation; however, there was no obvious EETs formation in lungs of PH mice, as suggested by negative H3Cit staining (Supplementary Figure 10). Therefore, we hypothesized that lipid mediators released by EOS may play a critical role in exerting the protective effects. EOS contain polyunsaturated fatty acid oxidation enzymes, making them the major site of lipid metabolism[6]. To get more insight into the pattern of lipid metabolism, EOS, $CD45^+$ cells (excluding EOS), and $CD45^-$ cells were sorted from lung cells of WT C57BL/6 mice by flow cytometry (Figure 7A). By determining the mRNA expression of enzymes in the COX and LOX pathways, we found that *Alox15* expression was 90 times higher in EOS than in other immune cells and 160 times higher than in $CD45^-$ cells (Figure 7A). Immunofluorescent staining showed that ALOX15 co-localized with $SiglecF^+$ cells in PH mouse lungs. No obvious $ALOX15^+$ staining was observed in the lung tissue of EOS-deficient ΔdblGATA mice (Figure 7B). Western blot analysis also revealed significantly lower ALOX15 expression in ΔdblGATA mouse lungs (Figure 7C) compared with WT lungs. Taken together, these results indicate that EOS are the main source of ALOX15.

UHPLC-MS/MS was then performed on lung tissues from WT and ΔdblGATA PH mice to identify the specific lipid mediators derived from EOS (Figure 7D and E). We found suppression of the 12/15-lipoxygenease pathway mediated by decreased ALOX15 expression in ΔdblGATA mouse lungs (Figure 7F-H). The concentrations of downstream oxylipins, such as 12-HETE (17.38±2.28 vs. 8.25±1.30 μg/g), 14-HDHA (2.64±0.41 vs. 1.29±0.24 μg/g), 17-HDHA (0.28±0.04 vs. 0.09±0.01 μg/g), and 15-HEPE (0.05±0.01 vs. 0.03±0.01 μg/g) were significantly lower in lung tissues from ΔdblGATA PH mice than in those from WT (Figure 7F-H). These decreases suggest that oxylipins from the 12/15-lipoxygenease pathway are mainly derived from EOS.

To further validate the function of oxylipins, 14-HDHA, 17-HDHA, 15-HEPE, and 12-HETE were chosen for *in vitro* PASMC proliferation assays (Figure 7I). We found that 14-HDHA, 17-HDHA, and 15-HEPE inhibited PDGFbb-induced proliferation in PASMCs at concentrations of 10 nM and 20 nM (Figure 7I); these effects were

consistent with those of EOS lysates and EOS supernatants (Figure 6). Moreover, 14-HDHA and 17-HDHA are the precursors of specialized pro-resolving mediators (SPM)[32], and they exhibit pro-resolving functions through membrane receptors, such as FPR2[33, 34]. ScRNA-seq showed that FPR2 was mainly expressed in neutrophils, monocytes, and macrophages (Supplementary Figure 11A and B), which was consistent with the observation that EOS deficiency promotes infiltration of neutrophils and monocytes/macrophages (Figure 5). By leukocyte adhesion and transmigration assay, we found that 14-HDHA and 17-HDHA treatment prevent neutrophil and monocyte/macrophage adhesion and migration. FPR2 inhibitor WRW4 pretreatment of neutrophils and monocytes/macrophages blocked the effect caused by 14/17-HDHA (Supplementary Figure 11C-F). In EOS-deletion PH mice, FPR2 agonist Ac2-26 administration mitigated the pro-inflammative effect caused by 14/17-HDHA shortage (Supplementary Figure 11G-I), suggesting the involvement of FPR2 in 14/17-HDHA mediated anti-inflammative effects.

Taken together, these results reveal that EOS exert anti-proliferative effects and anti-inflammative effects via oxylipins such as 14/17-HDHA produced by 12/15-lipoxygenease.

14/17-HDHA suppress PASMC proliferation by activating PPARγ

The anti-inflammatory effects of 14-HDHA and 17-HDHA have been widely reported[32]. We further investigated the mechanism underlying the anti-proliferative effect of 14/17-HDHA. As previously reported, 12/15-lipoxygenase metabolites regulate lipid metabolism by activating PPARγ[35], which is regarded as the major link between the TGFβ signaling and BMP2 signaling pathways during PAH development[36-38]. Once activated, PPARγ translocates into the nucleus and regulates downstream gene expression[36]. PPARγ activation also suppresses TGFβ-induced phosphorylation of Smad3 and Stat3[36]. These events together repress the proliferation of smooth muscle cells. Therefore, we speculated that EOS regulates PASMC homeostasis through PPARγ and that 14/17-HDHA participates in this process. To test this, we first monitored PPARγ activation in PASMCs. PDGFbb treatment reduced PPARγ translocation into the nucleus (Figure 8A, quantification in Supplementary Figure 12A) and enhanced Stat3 phosphorylation in PASMCs (Figure

8B, quantification in Supplementary Figure 12B). Treatment with EOS supernatants reversed the effects induced by PDGFbb, as shown by increased PPARγ nuclear location and decreased Stat3 phosphorylation (Figure 8A and B, Supplementary 12A and B). By contrast, Smad3 phosphorylation did not decrease under EOS supernatant treatment, excluding the role of Smad3 signaling in this process (Supplementary Figure 13). GW9662, an irreversible PPARγ antagonist, abolished the anti-proliferative effect of EOS supernatant treatment (Figure 8C). Also, downstream Stat3 phosphorylation increased when cells were treated with GW9662 (Figure 8D, quantification in Supplementary Figure 12C). Having identified 14-HDHA and 17-HDHA as EOS-derived mediators that suppress PASMC proliferation (Figure 7I), we then investigated whether 14/17-HDHA suppress PASMC proliferation through the PPARγ/Stat3 axis. PDGFbb-treated PASMCs were cultivated with 14-HDHA or 17-HDHA. We found that 14-HDHA and 17-HDHA treatment promoted PPARγ nuclear translocation and suppressed Stat3 phosphorylation (Figure 8E and F, quantification in Supplementary Figure 12D and E).

These observations suggest that EOS, whose downstream lipid mediators 14-HDHA and 17-HDHA promote PPARγ nuclear translocation, sustain PASMC homeostasis through PPARγ/Stat3.

Discussion

In this study, we found that EOS migrate from peripheral blood into lung tissue during PH development, and fibroblast-derived CCL11 might be responsible for EOS pulmonary recruitment. Furthermore, EOS deficiency aggravated PH, increased neutrophil and monocyte/macrophage infiltration, and promoted PASMC proliferation. We further demonstrated that EOS function through 12/15-lipoxygenease metabolites, and that downstream 14/17-HDHA mediates anti-inflammatory effects in immune cells through the SPM receptor FPR2, while inhibiting PASMC proliferation through PPARγ activation (Figure 8G).

Although the protective effects of EOS have been reported in many diseases, the underlying mechanisms vary[10, 11, 15, 16, 22-24]. In addition to the lipid mediators reported in our study and other studies, EOS granular proteins and cytokines have also been revealed to have protective effects in the progression of various diseases.

For example, in myocardial infarction and abdominal aortic aneurysm development, EOS were reported to function through Ear1 and IL4[10, 11], and through IL13 in liver injury[22]. However, these EOS-derived mediators also exist in other immune cells in lung tissue, suggesting that EOS are not the main source of these compounds: Ear1 is mainly secreted by alveolar macrophages[39, 40] and cytokines such as IL4 and IL13 are mainly derived from Th2 cells and mast cells[2, 3]. By contrast, the 12/15-lipoxygenase metabolites found in our study were uniquely expressed by EOS in lung tissues. EOS depletion largely repressed the production of lipid mediators in the lung, which participate in EOS-mediated PH development.

In our study, we identified 14-HDHA and 17-HDHA as the downstream lipid mediators produced by 12/15-lipoxygenase. The pro-resolving effect of 14-HDHA and 17-HDHA are well reported. Our study showed 14/17-HDHA suppressed inflammatory cell adhesion and migration through FPR2. Moreover, the scRNA-seq data showed that SPM receptor FPR2 was mainly expressed in neutrophils, macrophages, and monocytes, suggesting only these cells were capable of responding to EOS-derived SPM shortage in EOS-deletion mouse lungs. Besides, 14-HDHA and 17-HDHA are also the precursors of SPMs, such as protectins, resolvins, and maresins[32]. Although LS-MS/MS showed very low concentrations of these SPMs, we still cannot deny their effective roles in resolving inflammation.

Of note, we also showed that 14-HDHA and 17-HDHA exhibited an anti-proliferative effect on PDGFbb-induced PASMCs. 14-HDHA and 17-HDHA are lipid metabolites oxidized from docosahexaenoic acid. Lipid metabolites serve as the ligand of PPARγ[41]. These lipid ligands promoted PPARγ forming a heterodimer with retinoid X receptor (RXR), and subsequently binding to the peroxisome proliferator response element gene promoter[41]. This process has been documented for years, but mostly in metabolic syndromes[42]. In our study, we found that 14-HDHA and 17-HDHA promoted PPARγ activation and nuclear translocation in PASMCs. In PASMCs, activated PPARγ bound to Stat3 and inhibited Stat3 shuttling[36]. The same result could also be observed in 14/17-HDHA-activated PASMCs. 14/17-HDHA stimulation promotes PPARγ and blunts Stat3 phosphorylation, resulting in maintenance of PASMC homeostasis.

In the current study, we showed low levels of EOS in peripheral blood of PAH patients, SuHx-induced PH mice and rats, compared with control subjects/animals.

This could be due to an increase of EOS migration to lungs but no significant change of EOS generation in bone marrow. Thus, EOS maintained tissue homeostasis and played a protective role in lung. However, detrimental effects with high levels of EOS have been reported in pulmonary inflammation mouse models induced by OVA sensitization/challenge[43] or long-term IL-33 treatment[44]. Apparently, there are functional differences between the low and high EOS conditions, which might be due to the different EOS subtypes. Previous studies reported two EOS subtypes in lung tissue classified by CD101 expression, which are $CD101^-$ resident EOS and $CD101^+$ inflammatory EOS[20]. $CD101^-$ resident EOS were present in steady states, while $CD101^+$ inflammatory EOS were differentiated when receiving antigen stimulation (such as house dust mites or OVA)[15, 20]. In our study, there were no exogenous antigens applied in animal models and allergic diseases were excluded in enrolled human samples. We found no aberrant EOS generation in bone marrow, and $CD101^-$ resident EOS were the major functional subtype in bone marrow, blood and lungs. These resident EOS play a protective role in PH development. However, in those animal models with eosinophilia (high EOS levels), exogenous antigens or recombinant cytokines were used, which might affect EOS lineage maturation and differentiation. It warrants further investigation whether more EOS generation leads to eosinophilia and whether inflammatory EOS participate in disease development upon antigen stimulation. As resident EOS and inflammatory EOS are two subtypes with different functions, this may explain the functional differences between low and high EOS conditions. Of note, eosinophilia could also be observed in patients with COPD. Patients with eosinophilic COPD have a higher risk of PH onset[45]. Therefore, distinguishing the subtypes and specific functions of EOS between PAH patients (without allergic history) and COPD-PH patients (with eosinophilia) would benefit for revealing the function of EOS in different PH comprehensively.

The different EOS subtypes could also explain its different function in PH and asthma. PAH and asthma have been shown to share many pathophysiogical features, such as inflammation, vascular reactivity and structure remodeling[46]. EOS aggravated tissue damage in asthma[12], while EOS played a protective role in PAH. Previous study reported inflammatory EOS are the predominant subtype in OVA induced asthma mouse model[20], while in PH we revealed EOS infiltrated in lungs are mainly resident EOS (Supplementary Figure 1). Therefore, although similar, the pathophysiological heterogenicity of EOS needs to be evaluated in detail.

In PH development, EOS infiltration was also found in the RV of PH mice (Figure2H). RV hypertrophy and impairment also occurred in PH development; however, the role of EOS in RV hypertrophy remained unclear. A previous study reported the involvement of EOS in left ventricle function[11]. EOS protected cardiac function after acute myocardial infarction through decreasing cardiomyocyte death, cardiac fibrosis, and neutrophil adhesion[11]. Therefore, we speculate that EOS exhibit a similar function in the RV, which certainly deserves to be investigated experimentally in the future.

Despite we focused on EOS in current animal study, we do not exclude the possibility of the involvement of other myeloid cells and other cytokine signalings. For example, aberrant basophil lineage maturation was observed in a transgenic mouse line with EOS lineage ablation produced by genetically deleting GATA-1 promoter, which is because GATA-1 controls not only EOS but also other myeloid cells, such as basophils[47]. Thus, the effects observed in ΔdblGATA mice may be partially caused by basophil loss. Besides, in TRFK5-treated mice, neutralizing IL-5 arrested EOS maturation; however, IL-5 is not the only ligand for its receptor IL5RA (the β common cytokine receptor), IL-3 and GM-CSF also share the β common cytokine receptor[48, 49]. Thus, neutralizing IL-5 might free the IL5RA from IL-5 binding and subsequently enhance the signaling for IL-3 and GM-CSF binding. GM-CSF and IL-3 exhibit strong abilities in activating JAK/STAT signaling, and regulating chronic inflammation[49, 50]. Therefore, the observations in TRFK5-treated mice could be partially induced by GM-CSF and IL-3. Nevertheless, by using two different animal models (transgenic EOS deletion and pharmacal EOS depletion), we observed consistent results in mice and rats, suggesting the protective role of EOS in PH development. Further study with transgenic eosinophil-deficient mice (PHIL mice) or mice treated with neutralizing antibody against IL5RA would provide more comprehensive evidence for our conclusions.

Taken together, our study found that decreasing EOS with neutralizing IL5 subsequently aggravated PH development via 14/17-HDHA in animal models. Our study provided a proof-of-concept that clinical use of anti-IL5 monoclonal antibody (such as mepolizumab) might increase the risk of PH onset in patients. The mechanism (EOS-14/17-HDHA-FPR2/PPARγ axis) revealed in our study may suggest some other strategies in PAH treatment. For example, exogenous supplement

via food intake may compensate for 14/17-HDHA shortage in lung. Alternatively, targeting the downstream effective cells (such as neutrophils, monocytes and smooth muscle cells) could mimic the 14/17-HDHA function, similar to activating FPR2 by Ac2-26 and PPARγ by Rosiglitazone together to promote the resolution of inflammation and suppress the proliferation of PASMC in lung.

Author contributions

Ting Shu: Investigation, Methodology, Visualization, Writing - Original Draft
Jiawei Zhang: Investigation, Methodology, Visualization, Writing - Original Draft
Yitian Zhou: Software, Formal analysis, Data Curation, Visualization
Zhihua Chen: Supervision, Writing - Review & Editing
Jinqiu Li: Investigation, Validation, Visualization
Qihao Tang: Validation, Visualization
Wenqi Lei: Validation
Yanjiang Xing: Conceptualization, Supervision, Writing - Review & Editing, Project administration
Jing Wang: Conceptualization, Supervision, Writing - Review & Editing, Project administration, Funding acquisition
Chen Wang: Conceptualization, Supervision, Project administration, Funding acquisition

Sources of funding

This work was supported by the by CAMS Innovation Fund for Medical Sciences [2021-I2M-1-049 (J.W.), 2022-I2M-JB-007 (C.W.), 2021-I2M-1-005 (Y.X.), 2021-I2M-1-023 (T.S.)], Beijing Natural Science Foundation [Z220019 (J.W.)], Haihe Laboratory of Cell Ecosystem Innovation Fund [HH22KYZX0010 (J.W.)], the National Key Research and Development Program of China [2019YFA0802600 (J.W.)], the National Natural Science Foundation of China [81901588 (Y.X.)], the Non-profit Central Research Institute Fund of Chinese Academy of Medical Sciences [2019JB310001, 2018JB31001 (C.W.)], State Key Laboratory Special Fund [2060204 (C.W.)], and the Fundamental Research Funds for the Central Universities [3332022141 (J.Z.)].

Declaration of interests

No competing interests to declare.

Figure legend

Figure 1. Increased lung eosinophil (EOS) accumulation in PAH patients.

A. Blood EOS percentage of male/female PAH patients and sex-/age-matched healthy controls. (male non-PAH, n=31, male IPAH, n=30; female non-PAH, n=88, female IPAH, n=93) **B.** Blood EOS percentage of PAH patients in New York Heart Association (NYHA) functional class I/II and III/IV. (I/II, male:female=16:39; III/IV, male:female=14:54) **C.** Blood EOS percentage of non-mutant and *BMPR2* mutation-carried PAH patients. (non-mutation, n=52; mutation carrier, n=38.) **D.** Representative images of H&E and ECP immunohistochemical staining of lung sections from control subjects (non-PAH) or PAH patients. Scale bar=100 μm and 10 μm. **E.** Quantification of ECP positive cell number in lung section from human sample (n=5 for each group). **F**. Representative images of CD31 (green), α-SMA (yellow), Vimentin (blue) and ECP (red) immunofluorescent stainings of lung tissues from control subjects and PAH patients. Nuclei were counterstained with DAPI (white). Scale bar=100 μm and 25 μm. **G.** Lung mRNA expression of *IL5*, *CCL11*, *CCL24*, *CCL26* (n=5 per group). All data are shown as mean ± SEM. For A-C, E and G, differences were evaluated by unpaired two-tailed Student's *t*-test. **P*<0.05, ***P*<0.01.

Figure 2. Increased lung eosinophil (EOS) accumulation in PH mice.

A. Flow cytometric analyses of $CD11b^+SiglecF^+$ EOS among $CD45^+$ cells in peripheral blood of control or PH mice. **B.** Flow cytometric analyses of $CD11b^+SiglecF^+$ EOS among $CD45^+$ cells in lung tissues of control or PH mice (n=8 per group). **C.** Representative images of H&E and SiglecF immunofluorescent staining of lung sections from control and PH mice (left panel, scale bar=25 μm) and quantification of EOS number in lung section (right panel, n=4 per group). **D.** Lung mRNA expression of *Il5*, *Ccl11*, *Ccl24*, and *Ccl26* (n=5 per group). **E.** Lung IL5 and CCL11 protein levels of control or PH mice (n=5 per group). **F.** The percentage of EOS among $CD45^+$ cells in bone marrows of control or PH mice (n=8 per group). **G.**

The percentage of EOS among $CD45^+$ cells in spleens of control or PH mice (n=8 per group). **H.** The percentage of EOS among $CD45^+$ cells in right ventricles of control or PH mice (n=6 per group). **I.** The percentage of EOS among $CD45^+$ cells in left ventricles of control or PH mice (n=6 per group). All data are shown as mean ± SEM. Differences were analysed by unpaired two-tailed Student's *t*-test. **P*<0.05, ***P*<0.01, ****P*<0.001, ns, no significance.

Figure 3. CCL11 expression in pulmonary adventitial fibroblasts.

A. Dot plots of gene expression (*IL5*, *CCL11*, *CCL24*, and *CCL26*) among cell clusters in human. **B.** Dot plots of gene expression (*Il5*, *Ccl11*, *Ccl24*, and *Ccl26*) among cell clusters in mouse. **C.** Violin plots of the expression of *Ccl11* among two subgroups of fibroblasts in control and PH mice lung tissues. **D.** Representative images of CCL11 and PDGFRa immunofluorescent staining of the lung sections from control subjects (non-PAH) or PAH patients. Scale bar=25 μm. **E.** Representative images of CCL11 and PDGFRa immunofluorescent staining of the lung sections from control or PH mice. Scale bar=25 μm. **F.** Relative mRNA expression of *CCL11* in human PAF under different treatments (n=3 for three independent repeats). **G.** Relative mRNA expression of *Ccl11* in mouse PAF under different conditions (n=3 for three independent repeats). **H**. Representative images and quantification of EOS adhesive assay. Green arrow pointing at the 5-(and 6)-carboxyfluorescein diacetate succinimidyl ester (CFSE)-labeled EOS (green). Scale bar=100 μm. All data are shown as mean ± SEM. Differences were evaluated by unpaired two-tail Student's *t*-test. **P*<0.05, ****P*<0.001, *****P*<0.0001, ns, no significance.

Figure 4. EOS deficiency and depletion exacerbate PH in mice.

A. Strategy for SuHx-induced PH in wildtype (WT) or EOS-deficient (ΔdblGATA) male mice (control: n=4 per group; SuHx: n=7 for WT, n=9 for ΔdblGATA). **B.** Representative flow cytometric analyses of $CD11b^+SiglecF^+$ EOS among $CD45^+$ cells in lung tissues of WT or ΔdblGATA mice. **C.** The percentage of EOS among $CD45^+$ cells in lung tissues of WT or ΔdblGATA mice. **D.** Right ventricular systolic pressure (RVSP) of WT and ΔdblGATA mice. **E.** RV/LV+S of the different experimental groups. **F.** Representative images of α-SMA and CD31 immunofluorescent staining of the lung sections from WT or ΔdblGATA mice. Scale bar=25 μm. **G.** Quantification

of pulmonary vascular medial thickness to total cross sectional area (CSA), for vessels of 20-50 μm and 50-100 μm in diameter, respectively. **H.** Proportion of non-muscularized (N), partially muscularized (P), or full muscularized (F) pulmonary vessels of 20-100 μm in diameter. **I.** Strategy for SuHx-induced PH in male mice injected with isotype control antibody or TRFK5 (control: n=5 per group; SuHx: n=8 per group). **J.** Representative flow cytometric analyses of $CD11b^+SiglecF^+$ EOS among $CD45^+$ cells in lung tissues of isotype control or TRFK5 treated mice. **K.** The percentage of EOS among $CD45^+$ cells in lung tissues of isotype control or TRFK5 treated mice. **L.** RVSP of isotype control or TRFK5 treated mice. **M.** RV/LV+S of the different experimental groups. **N.** Representative images of α-SMA and CD31 immunofluorescent staining of the lung sections from isotype control or TRFK5 treated mice. Scale bar=25 μm. **O.** Quantification of wall thickness of the pulmonary vasculature, for vessels of 20-50 μm and 50-100 μm in diameter, respectively. **P.** Proportion of non-muscularized (N), partially muscularized (P), or full muscularized (F) pulmonary vessels of 20-100 μm in diameter. All data are shown as mean ± SEM. Differences between multiple groups were evaluated by two-way ANOVA with Bonferroni's post hoc test. **P*<0.05, ***P*<0.01, ****P*<0.001 and *****P*<0.0001 for ΔdblGATA versus WT mice, or TRFK5 versus isotype control-treated mice; $^{\#}P$<0.05, $^{\#\#}P$<0.01, $^{\#\#\#}P$<0.001 $^{\#\#\#\#}P$<0.0001 for mice in control versus SuHx groups.

Figure 5. EOS deficiency or depletion promotes neutrophil and monocyte/macrophage accumulation in lung.

A. Representative flow cytometric analyses of $CD11b^+Ly6G^+$ neutrophils among $CD45^+$ cells in lung tissues of WT or ΔdblGATA male mice (left panel) and the percentage of neutrophils among $CD45^+$ cells (right panel). **B.** Representative flow cytometric analyses of $CD11b^+Ly6C^+$ monocytes/macrophages among $CD45^+$ cells in lung tissues of WT or ΔdblGATA male mice (left panel) and the percentage of monocytes/macrophages among $CD45^+$ cells (right panel). **C.** Representative images of Ly6G and α-SMA immunofluorescent staining of lung sections from WT or ΔdblGATA male mice (left panel) and quantification of $Ly6G^+$ cell numbers per mm^2 lung tissue (right panel). Scale bar=50 μm. **D.** Representative images of CD68 and α-SMA immunofluorescent staining of lung sections from WT or ΔdblGATA male mice (left panel) and quantification of $CD68^+$ cell numbers per mm^2 lung tissue (right panel). Scale bar=50 μm. **E.** Representative flow cytometric analyses of

$CD11b^+Ly6G^+$ neutrophils among $CD45^+$ cells in lung tissues of isotype control or TRFK5 treated male mice (left panel) and the percentage of neutrophils among $CD45^+$ cells (right panel). **F.** Representative flow cytometric analyses of $CD11b^+Ly6C^+$ monocytes/macrophages among $CD45^+$ cells in lung tissues of isotype control or TRFK5 treated male mice (left panel) and the percentage of $CD11b^+Ly6C^+$monocytes/macrophages among $CD45^+$ cells (right panel). **G.** Representative images of Ly6G and α-SMA immunofluorescent staining of lung sections from isotype control or TRFK5 treated male mice (left panel) and quantification of $Ly6G^+$ cell numbers per mm^2 lung tissue (right panel). Scale bar=50 μm. **H.** Representative images of CD68 and α-SMA immunofluorescent staining of lung sections from isotype control or TRFK5 treated male mice (left panel) and quantification of $CD68^+$ cell numbers per mm^2 lung tissue (right panel). Scale bar=50 μm. Differences between multiple groups were evaluated by two-way ANOVA with Bonferroni's post hoc test. For **A-D**, control: n=4 per group; SuHx: n=7 for WT, n=9 for ΔdblGATA. For **E-H**, control: n=5 for isotype control, n=4 for TRFK5; SuHx: n=8 per group. All data are shown as mean ± SEM. $*P<0.05$, $**P<0.01$ and for ΔdblGATA versus WT mice, or TRFK5 versus isotype control-treated mice; $^{\#}P<0.05$ and $^{\#\#}P<0.01$ for mice in control versus SuHx groups.

Figure 6. EOS abolishes PDGFbb-induced smooth muscle cell proliferation and migration.

A. Strategy for *in vitro* experiments. **B.** Representative flow cytometric identification (left panel) and Wright-Giemsa staining (right panel) of liquid-cultured bone-marrow-derived EOS. Scale bar=10 μm. **C.** The percentage of mouse PASMC proliferation after treatment of PDGFbb (10 ng/mL) and different concentrations of EOS lysate (equivalent to 1×10^3, 1×10^4, 1×10^5, 1×10^6 EOS per mL) for 24 h compared with untreated control. **D.** Representative images of wound-healing (upper panel) and Boyden Chamber migration assay (down panel) for mouse PASMC after treatment of PDGFbb (10 ng/mL) and different concentrations of EOS lysate (equivalent to 1×10^3, 1×10^4, 1×10^5, 1×10^6 EOS per mL) for 24 h. Scale bar=250 μm. **E.** The percentage of mouse PASMC proliferation after treatment of PDGFbb (10 ng/mL) and different concentrations of EOS supernatant (equivalent to 1×10^3, 1×10^4, 1×10^5, 1×10^6 EOS per mL) for 24 h compared with untreated control, measured by CCK8. **F.** Representative images of wound-healing (upper panel) and Boyden

Chamber migration assay (down panel) for mouse PASMC after treatment of PDGFbb (10 ng/mL) and different concentrations of EOS supernatant (equivalent to 1×10^3, 1×10^4, 1×10^5, 1×10^6 EOS per mL) for 24 h. Scale bar=250 μm. **G.** The percentage of wound closure (left panel) and quantification of migrated PASMC (right panel) in **D**. **H.** The percentage of wound closure (left panel) and quantification of migrated PASMC (right panel) in **F**. All data are shown as mean ± SEM. Differences were evaluated by one-way ANOVA with Bonferroni's post hoc test. $^{\#}P<0.05$, $^{\#\#\#\#}P<0.0001$ for PDGFbb-treated group compared with untreated-control group; $^{**}P<0.01$, $^{***}P<0.001$, $^{****}P<0.0001$, ns, no significance for EOS-lysate/supernatant -treated groups versus PDGFbb-treated groups.

Figure 7. 12/15-lipoxygenase derivatives deficiency in lungs of ΔdblGATA mice.
A. Strategy for flow cytometric sorting from lung tissues of C57/BL6 mice (top panel) and relative mRNA expression of *Alox5, Alox12, Alox15, Cox1* and *Cox2* in sorted cells (bottom panel, n=3). **B.** Representative images of Alox15 and SiglecF immunofluorescent staining of lung sections from WT or ΔdblGATA mice. Scale bar=25 and 100 μm. **C.** Representative western blots (top panel) and quantification (bottom panel) of Alox15 in the lungs of WT and ΔdblGATA mice with PH (n=6 per group). **D.** Principal component analysis of lipidomics data. **E.** Heatmap showing key lipid derivatives differentially expressed in lung tissues of WT or ΔdblGATA mice with PH (n=9 per group). **F.** Quantification of Arachidonic acid (AA)-derived products in lung tissues of WT and ΔdblGATA mice with PH (n=9 per group). **G.** Quantification of Docosahexaenoic acid (DHA)-derived products in lung tissues of WT and ΔdblGATA mice with PH (n=9 per group). **H.** Quantification of Eicosapentaenoic acid (EPA)-derived products in lung tissues of WT and ΔdblGATA mice with PH (n=9 per group). **I.** The percentage of mouse PASMC proliferation after treatment of PDGFbb (10 ng/mL) and different concentrations of 12/15-LOX derivatives (5 nM, 10 nM, 20 nM, 100 nM) compared with untreated control, measured by CCK8. For A and I, differences between groups were evaluated by one-way ANOVA with Bonferroni's post hoc test. For C, F-H, differences were evaluated by unpaired two-tailed Student's *t*-test. All data are shown as mean ± SEM. $^{\#}P<0.05$, $^{\#\#}P<0.01$ for PDGFbb-treated group compared with untreated-control group, $^{*}P<0.05$, $^{**}P<0.01$, $^{***}P<0.001$, $^{****}P<0.0001$ for 12/15-LOX derivatives-treated groups versus PDGFbb-treated groups, or WT versus ΔdblGATA mice with PH, ns, no

significance, ND, not detected.

Figure 8. EOS-derived 14/17-HDHA inhibits PASMC proliferation via activating PPARγ.

A.Representative western blots of PPARγ in cytoplasmic and nuclear extracts of mouse PASMC treated with PDGFbb and different concentrations of EOS supernatant (equivalent to 1×10^4, 1×10^5, 1×10^6 EOS per mL) for 24 h (n=3). **B.** Representative western blots of Stat3 and pStat3 in cytoplasmic and nuclear extracts of mouse PASMC treated with PDGFbb (10 ng/mL) and different concentrations of EOS supernatant (equivalent to 1×10^4, 1×10^5, 1×10^6 EOS per mL) for 24 h (n=3). **C.** The percentage of mouse PASMC proliferation pre-incubated with GW9662 (1 μM) or DMSO for 24 h, then treated with PDGFbb (10 ng/mL) and EOS supernatant (equivalent to 1×10^5 EOS per mL) for another 24 h compared with untreated control. **D.** Representative western blots of Stat3 and pStat3 in cytoplasmic and nuclear extracts of mouse PASMC pre-incubated with GW9662 or DMSO for 24 h, then treated with PDGFbb and EOS supernatant (equivalent to 1×10^5 EOS per mL) for another 24 h (n=3). **E.** Representative western blots of PPARγ in cytoplasmic and nuclear extracts of mouse PASMC treated with PDGFbb and 14-HDHA, 17-HDHA (10 nM) for 24 h (n=3). **F.** Representative western blots of Stat3 and pStat3 in cytoplasmic and nuclear extracts of mouse PASMC treated with PDGFbb and 14-HDHA, 17-HDHA (10 nM) for 24 h (n=3). **G.** Schematic representation of the proposed mechanism underlying EOS-mediated protection in PH. For C, differences between groups were evaluated by one-way ANOVA with Bonferroni's post hoc test. $^{\#\#\#\#}P<0.0001$ for PDGFbb-treated group compared with untreated-control group, $****P<0.0001$ for other groups vs. EOS supernatant-treated groups.

References

1. Humbert M, Guignabert C, Bonnet S, Dorfmuller P, Klinger JR, Nicolls MR, Olschewski AJ, Pullamsetti SS, Schermuly RT, Stenmark KR, Rabinovitch M. Pathology and pathobiology of pulmonary hypertension: state of the art and research perspectives. *Eur Respir J* 2019: 53(1).

2. Daley E, Emson C, Guignabert C, de Waal Malefyt R, Louten J, Kurup VP, Hogaboam C, Taraseviciene-Stewart L, Voelkel NF, Rabinovitch M, Grunig E, Grunig

G. Pulmonary arterial remodeling induced by a Th2 immune response. *J Exp Med* 2008: 205(2): 361-372.

3. Chen G, Zuo S, Tang J, Zuo C, Jia D, Liu Q, Liu G, Zhu Q, Wang Y, Zhang J, Shen Y, Chen D, Yuan P, Qin Z, Ruan C, Ye J, Wang XJ, Zhou Y, Gao P, Zhang P, Liu J, Jing ZC, Lu A, Yu Y. Inhibition of CRTH2-mediated Th2 activation attenuates pulmonary hypertension in mice. *J Exp Med* 2018: 215(8): 2175-2195.

4. Lambrecht BN, Hammad H. The immunology of asthma. *Nat Immunol* 2015: 16(1): 45-56.

5. Harbaum L, Baaske KM, Simon M, Oqueka T, Sinning C, Glatzel A, Luneburg N, Sydow K, Bokemeyer C, Klose H. Exploratory analysis of the neutrophil to lymphocyte ratio in patients with pulmonary arterial hypertension. *BMC Pulm Med* 2017: 17(1): 72.

6. Stone KD, Prussin C, Metcalfe DD. IgE, mast cells, basophils, and eosinophils. *J Allergy Clin Immunol* 2010: 125(2 Suppl 2): S73-80.

7. Grisaru-Tal S, Itan M, Klion AD, Munitz A. A new dawn for eosinophils in the tumour microenvironment. *Nat Rev Cancer* 2020: 20(10): 594-607.

8. Ramirez GA, Yacoub MR, Ripa M, Mannina D, Cariddi A, Saporiti N, Ciceri F, Castagna A, Colombo G, Dagna L. Eosinophils from Physiology to Disease: A Comprehensive Review. *Biomed Res Int* 2018: 2018: 9095275.

9. Weller PF, Spencer LA. Functions of tissue-resident eosinophils. *Nat Rev Immunol* 2017: 17(12): 746-760.

10. Liu CL, Liu X, Zhang Y, Liu J, Yang C, Luo S, Liu T, Wang Y, Lindholt JS, Diederichsen A, Rasmussen LM, Dahl M, Sukhova GK, Lu G, Upchurch GR, Libby P, Guo J, Zhang J, Shi GP. Eosinophils Protect Mice From Angiotensin-II Perfusion-Induced Abdominal Aortic Aneurysm. *Circ Res* 2021: 128(2): 188-202.

11. Liu J, Yang C, Liu T, Deng Z, Fang W, Zhang X, Li J, Huang Q, Liu C, Wang Y, Yang D, Sukhova GK, Lindholt JS, Diederichsen A, Rasmussen LM, Li D, Newton G, Luscinskas FW, Liu L, Libby P, Wang J, Guo J, Shi GP. Eosinophils improve cardiac function after myocardial infarction. *Nat Commun* 2020: 11(1): 6396.

12. Lu Y, Huang Y, Li J, Huang J, Zhang L, Feng J, Li J, Xia Q, Zhao Q, Huang L, Jiang S, Su S. Eosinophil extracellular traps drive asthma progression through neuro-immune signals. *Nat Cell Biol* 2021: 23(10): 1060-1072.

13. Marx C, Novotny J, Salbeck D, Zellner KR, Nicolai L, Pekayvaz K, Kilani B,

Stockhausen S, Burgener N, Kupka D, Stocker TJ, Weckbach LT, Pircher J, Moser M, Joner M, Desmet W, Adriaenssens T, Neumann FJ, Gerschlick AH, Ten Berg JM, Lorenz M, Stark K. Eosinophil-platelet interactions promote atherosclerosis and stabilize thrombosis with eosinophil extracellular traps. *Blood* 2019: 134(21): 1859-1872.

14. Choi Y, Le Pham D, Lee DH, Lee SH, Kim SH, Park HS. Biological function of eosinophil extracellular traps in patients with severe eosinophilic asthma. *Exp Mol Med* 2018: 50(8): 1-8.

15. Zhu C, Weng QY, Zhou LR, Cao C, Li F, Wu YF, Wu YP, Li M, Hu Y, Shen JX, Xiong XF, Lan F, Xia LX, Zhang B, Zhang H, Huang M, Ying SM, Shen HH, Chen ZH, Li W. Homeostatic and early-recruited CD101(-) eosinophils suppress endotoxin-induced acute lung injury. *Eur Respir J* 2020: 56(5).

16. Masterson JC, McNamee EN, Fillon SA, Hosford L, Harris R, Fernando SD, Jedlicka P, Iwamoto R, Jacobsen E, Protheroe C, Eltzschig HK, Colgan SP, Arita M, Lee JJ, Furuta GT. Eosinophil-mediated signalling attenuates inflammatory responses in experimental colitis. *Gut* 2015: 64(8): 1236-1247.

17. Galdiero MR, Varricchi G, Seaf M, Marone G, Levi-Schaffer F, Marone G. Bidirectional Mast Cell-Eosinophil Interactions in Inflammatory Disorders and Cancer. *Front Med (Lausanne)* 2017: 4: 103.

18. Wong TW, Doyle AD, Lee JJ, Jelinek DF. Eosinophils regulate peripheral B cell numbers in both mice and humans. *J Immunol* 2014: 192(8): 3548-3558.

19. Singh G, Brass A, Knight CG, Cruickshank SM. Gut eosinophils and their impact on the mucus-resident microbiota. *Immunology* 2019: 158(3): 194-205.

20. Mesnil C, Raulier S, Paulissen G, Xiao X, Birrell MA, Pirottin D, Janss T, Starkl P, Ramery E, Henket M, Schleich FN, Radermecker M, Thielemans K, Gillet L, Thiry M, Belvisi MG, Louis R, Desmet C, Marichal T, Bureau F. Lung-resident eosinophils represent a distinct regulatory eosinophil subset. *J Clin Invest* 2016: 126(9): 3279-3295.

21. Acharya KR, Ackerman SJ. Eosinophil granule proteins: form and function. *J Biol Chem* 2014: 289(25): 17406-17415.

22. Wang Y, Yang Y, Wang M, Wang S, Jeong JM, Xu L, Wen Y, Emontzpohl C, Atkins CL, Duong K, Moreno NF, Yuan X, Hall DR, Dar W, Feng D, Gao B, Xu Y, Czigany Z, Colgan SP, Bynon JS, Akira S, Brown JM, Eltzschig HK, Jacobsen EA, Ju

C. Eosinophils attenuate hepatic ischemia-reperfusion injury in mice through ST2-dependent IL-13 production. *Sci Transl Med* 2021: 13(579).

23. Brigger D, Riether C, van Brummelen R, Mosher KI, Shiu A, Ding Z, Zbaren N, Gasser P, Guntern P, Yousef H, Castellano JM, Storni F, Graff-Radford N, Britschgi M, Grandgirard D, Hinterbrandner M, Siegrist M, Moullan N, Hofstetter W, Leib SL, Villiger PM, Auwerx J, Villeda SA, Wyss-Coray T, Noti M, Eggel A. Eosinophils regulate adipose tissue inflammation and sustain physical and immunological fitness in old age. *Nat Metab* 2020: 2(8): 688-702.

24. Wu D, Molofsky AB, Liang HE, Ricardo-Gonzalez RR, Jouihan HA, Bando JK, Chawla A, Locksley RM. Eosinophils sustain adipose alternatively activated macrophages associated with glucose homeostasis. *Science* 2011: 332(6026): 243-247.

25. Galie N, Humbert M, Vachiery JL, Gibbs S, Lang I, Torbicki A, Simonneau G, Peacock A, Vonk Noordegraaf A, Beghetti M, Ghofrani A, Gomez Sanchez MA, Hansmann G, Klepetko W, Lancellotti P, Matucci M, McDonagh T, Pierard LA, Trindade PT, Zompatori M, Hoeper M, Group ESCSD. 2015 ESC/ERS Guidelines for the diagnosis and treatment of pulmonary hypertension: The Joint Task Force for the Diagnosis and Treatment of Pulmonary Hypertension of the European Society of Cardiology (ESC) and the European Respiratory Society (ERS): Endorsed by: Association for European Paediatric and Congenital Cardiology (AEPC), International Society for Heart and Lung Transplantation (ISHLT). *Eur Heart J* 2016: 37(1): 67-119.

26. Galie N, McLaughlin VV, Rubin LJ, Simonneau G. An overview of the 6th World Symposium on Pulmonary Hypertension. *Eur Respir J* 2019: 53(1).

27. Ciuclan L, Bonneau O, Hussey M, Duggan N, Holmes AM, Good R, Stringer R, Jones P, Morrell NW, Jarai G, Walker C, Westwick J, Thomas M. A novel murine model of severe pulmonary arterial hypertension. *Am J Respir Crit Care Med* 2011: 184(10): 1171-1182.

28. Garlisi CG, Kung TT, Wang P, Minnicozzi M, Umland SP, Chapman RW, Stelts D, Crawley Y, Falcone A, Myers JG, Jones H, Billah MM, Kreutner W, Egan RW. Effects of chronic anti-interleukin-5 monoclonal antibody treatment in a murine model of pulmonary inflammation. *Am J Respir Cell Mol Biol* 1999: 20(2): 248-255.

29. Morrell NW, Aldred MA, Chung WK, Elliott CG, Nichols WC, Soubrier F,

Trembath RC, Loyd JE. Genetics and genomics of pulmonary arterial hypertension. *Eur Respir J* 2019: 53(1).

30. Ortega HG, Liu MC, Pavord ID, Brusselle GG, FitzGerald JM, Chetta A, Humbert M, Katz LE, Keene ON, Yancey SW, Chanez P, Investigators M. Mepolizumab treatment in patients with severe eosinophilic asthma. *N Engl J Med* 2014: 371(13): 1198-1207.

31. Klion AD, Ackerman SJ, Bochner BS. Contributions of Eosinophils to Human Health and Disease. *Annu Rev Pathol* 2020: 15: 179-209.

32. Gabbs M, Leng S, Devassy JG, Monirujjaman M, Aukema HM. Advances in Our Understanding of Oxylipins Derived from Dietary PUFAs. *Adv Nutr* 2015: 6(5): 513-540.

33. Serhan CN. Pro-resolving lipid mediators are leads for resolution physiology. *Nature* 2014: 510(7503): 92-101.

34. Liu GJ, Tao T, Wang H, Zhou Y, Gao X, Gao YY, Hang CH, Li W. Functions of resolvin D1-ALX/FPR2 receptor interaction in the hemoglobin-induced microglial inflammatory response and neuronal injury. *J Neuroinflammation* 2020: 17(1): 239.

35. Sun L, Xu YW, Han J, Liang H, Wang N, Cheng Y. 12/15-Lipoxygenase metabolites of arachidonic acid activate PPARgamma: a possible neuroprotective effect in ischemic brain. *J Lipid Res* 2015: 56(3): 502-514.

36. Calvier L, Chouvarine P, Legchenko E, Hoffmann N, Geldner J, Borchert P, Jonigk D, Mozes MM, Hansmann G. PPARgamma Links BMP2 and TGFbeta1 Pathways in Vascular Smooth Muscle Cells, Regulating Cell Proliferation and Glucose Metabolism. *Cell Metab* 2017: 25(5): 1118-1134 e1117.

37. Legchenko E, Chouvarine P, Borchert P, Fernandez-Gonzalez A, Snay E, Meier M, Maegel L, Mitsialis SA, Rog-Zielinska EA, Kourembanas S, Jonigk D, Hansmann G. PPARgamma agonist pioglitazone reverses pulmonary hypertension and prevents right heart failure via fatty acid oxidation. *Sci Transl Med* 2018: 10(438).

38. Hennigs JK, Cao A, Li CG, Shi M, Mienert J, Miyagawa K, Korbelin J, Marciano DP, Chen PI, Roughley M, Elliott MV, Harper RL, Bill MA, Chappell J, Moonen JR, Diebold I, Wang L, Snyder MP, Rabinovitch M. PPARgamma-p53-Mediated Vasculoregenerative Program to Reverse Pulmonary Hypertension. *Circ Res* 2021: 128(3): 401-418.

39. Cormier SA, Yuan S, Crosby JR, Protheroe CA, Dimina DM, Hines EM, Lee NA,

Lee JJ. T(H)2-mediated pulmonary inflammation leads to the differential expression of ribonuclease genes by alveolar macrophages. *Am J Respir Cell Mol Biol* 2002: 27(6): 678-687.

40. Luo M, Lai W, He Z, Wu L. Development of an Optimized Culture System for Generating Mouse Alveolar Macrophage-like Cells. *J Immunol* 2021: 207(6): 1683-1693.

41. Marion-Letellier R, Dechelotte P, Iacucci M, Ghosh S. Dietary modulation of peroxisome proliferator-activated receptor gamma. *Gut* 2009: 58(4): 586-593.

42. Lodhi IJ, Semenkovich CF. Peroxisomes: a nexus for lipid metabolism and cellular signaling. *Cell Metab* 2014: 19(3): 380-392.

43. Weng M, Baron DM, Bloch KD, Luster AD, Lee JJ, Medoff BD. Eosinophils are necessary for pulmonary arterial remodeling in a mouse model of eosinophilic inflammation-induced pulmonary hypertension. *Am J Physiol Lung Cell Mol Physiol* 2011: 301(6): L927-936.

44. Ikutani M, Tsuneyama K, Kawaguchi M, Fukuoka J, Kudo F, Nakae S, Arita M, Nagai Y, Takaki S, Takatsu K. Prolonged activation of IL-5-producing ILC2 causes pulmonary arterial hypertrophy. *JCI Insight* 2017: 2(7): e90721.

45. Alzghoul BN, As Sayaideh M, Moreno BF, Singh SK, Innabi A, Reddy R, Papierniak ES, Alnuaimat HM. Pulmonary hypertension in eosinophilic versus noneosinophilic COPD. *ERJ Open Res* 2021: 7(1).

46. Said SI, Hamidi SA, Gonzalez Bosc L. Asthma and pulmonary arterial hypertension: do they share a key mechanism of pathogenesis? *Eur Respir J* 2010: 35(4): 730-734.

47. Nei Y, Obata-Ninomiya K, Tsutsui H, Ishiwata K, Miyasaka M, Matsumoto K, Nakae S, Kanuka H, Inase N, Karasuyama H. GATA-1 regulates the generation and function of basophils. *Proc Natl Acad Sci U S A* 2013: 110(46): 18620-18625.

48. Nelson RK, Brickner H, Panwar B, Ramirez-Suastegui C, Herrera-de la Mata S, Liu N, Diaz D, Alexander LEC, Ay F, Vijayanand P, Seumois G, Akuthota P. Human Eosinophils Express a Distinct Gene Expression Program in Response to IL-3 Compared with Common beta-Chain Cytokines IL-5 and GM-CSF. *J Immunol* 2019: 203(2): 329-337.

49. Dougan M, Dranoff G, Dougan SK. GM-CSF, IL-3, and IL-5 Family of Cytokines: Regulators of Inflammation. *Immunity* 2019: 50(4): 796-811.

50. Sawada H, Saito T, Nickel NP, Alastalo TP, Glotzbach JP, Chan R, Haghighat L, Fuchs G, Januszyk M, Cao A, Lai YJ, Perez Vde J, Kim YM, Wang L, Chen PI, Spiekerkoetter E, Mitani Y, Gurtner GC, Sarnow P, Rabinovitch M. Reduced BMPR2 expression induces GM-CSF translation and macrophage recruitment in humans and mice to exacerbate pulmonary hypertension. *J Exp Med* 2014: 211(2): 263-280.

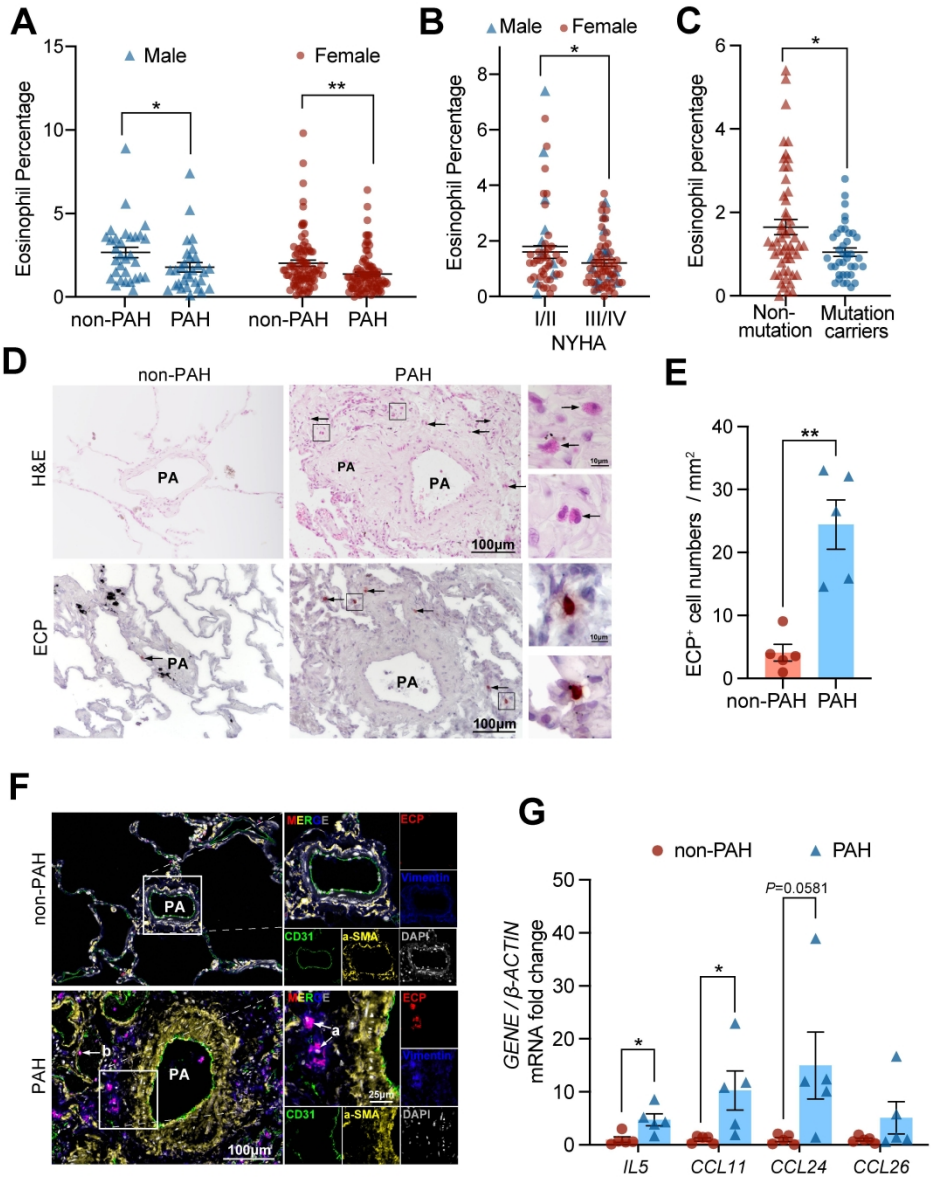

Figure 1. Increased lung eosinophil (EOS) accumulation in PAH patients.
A.Blood EOS percentage of male/female PAH patients and sex-/age-matched healthy controls. (male non-PAH, n=31, male IPAH, n=30; female non-PAH, n=88, female IPAH, n=93) B. Blood EOS percentage of PAH patients in New York Heart Association (NYHA) functional class I/II and III/IV. (I/II, male:female=16:39; III/IV, male:female=14:54) C. Blood EOS percentage of non-mutant and BMPR2 mutation-carried PAH patients. (non-mutation, n=52; mutation carrier, n=38.) D. Representative images of H&E and ECP immunohistochemical staining of lung sections from control subjects (non-PAH) or PAH patients. Scale bar=100 μm and 10 μm. E. Quantification of ECP positive cell number in lung section from human sample (n=5 for each group). F. Representative images of CD31 (green), α-SMA (yellow), Vimentin (blue) and ECP (red) immunofluorescent stainings of lung tissues from control subjects and PAH patients. Nuclei were counterstained with DAPI (white). Scale bar=100 μm and 25 μm. G. Lung mRNA expression of IL5, CCL11, CCL24, CCL26 (n=5 per group). All data are shown as mean ± SEM. For A-C, E and G, differences were evaluated by unpaired two-tailed Student's t-test. *P<0.05, **P<0.01.

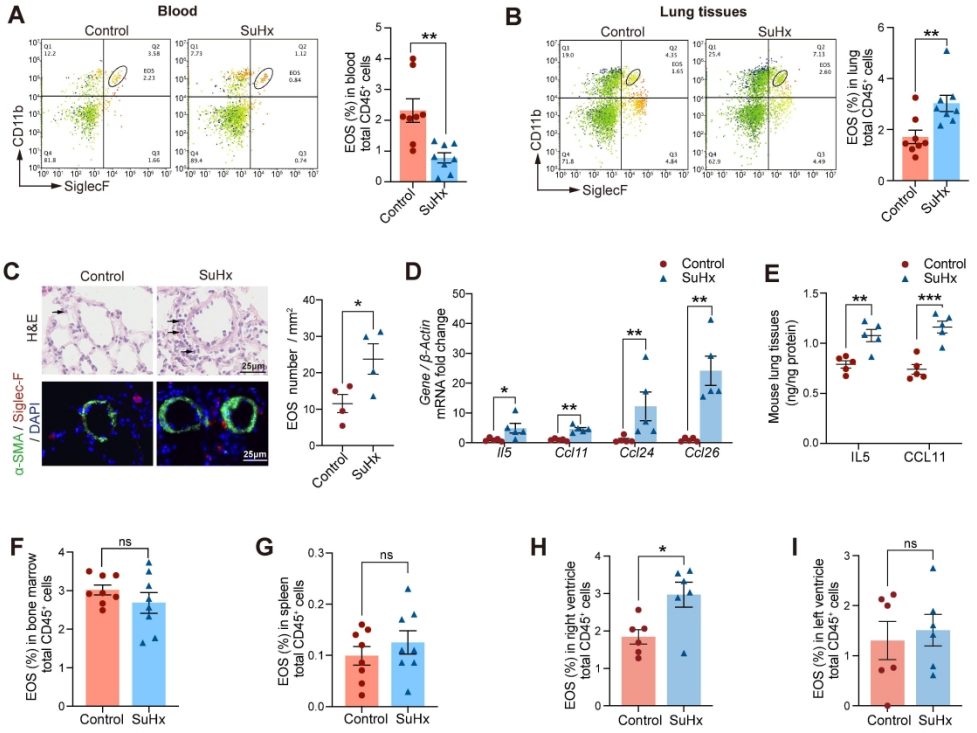

Figure 2. Increased lung eosinophil (EOS) accumulation in PH mice.
A.Flow cytometric analyses of CD11b+SiglecF+ EOS among CD45+ cells in peripheral blood of control or PH mice. B. Flow cytometric analyses of CD11b+SiglecF+ EOS among CD45+ cells in lung tissues of control or PH mice (n=8 per group). C. Representative images of H&E and SiglecF immunofluorescent staining of lung sections from control and PH mice (left panel, scale bar=25 μm) and quantification of EOS number in lung section (right panel, n=4 per group). D. Lung mRNA expression of Il5, Ccl11, Ccl24, and Ccl26 (n=5 per group). E. Lung IL5 and CCL11 protein levels of control or PH mice (n=5 per group). F. The percentage of EOS among CD45+ cells in bone marrows of control or PH mice (n=8 per group). G. The percentage of EOS among CD45+ cells in spleens of control or PH mice (n=8 per group). H. The percentage of EOS among CD45+ cells in right ventricles of control or PH mice (n=6 per group). I. The percentage of EOS among CD45+ cells in left ventricles of control or PH mice (n=6 per group). All data are shown as mean ± SEM. Differences were analysed by unpaired two-tailed Student's t-test. *P<0.05, **P<0.01, ***P<0.001, ns, no significance.

180x134mm (600 x 600 DPI)

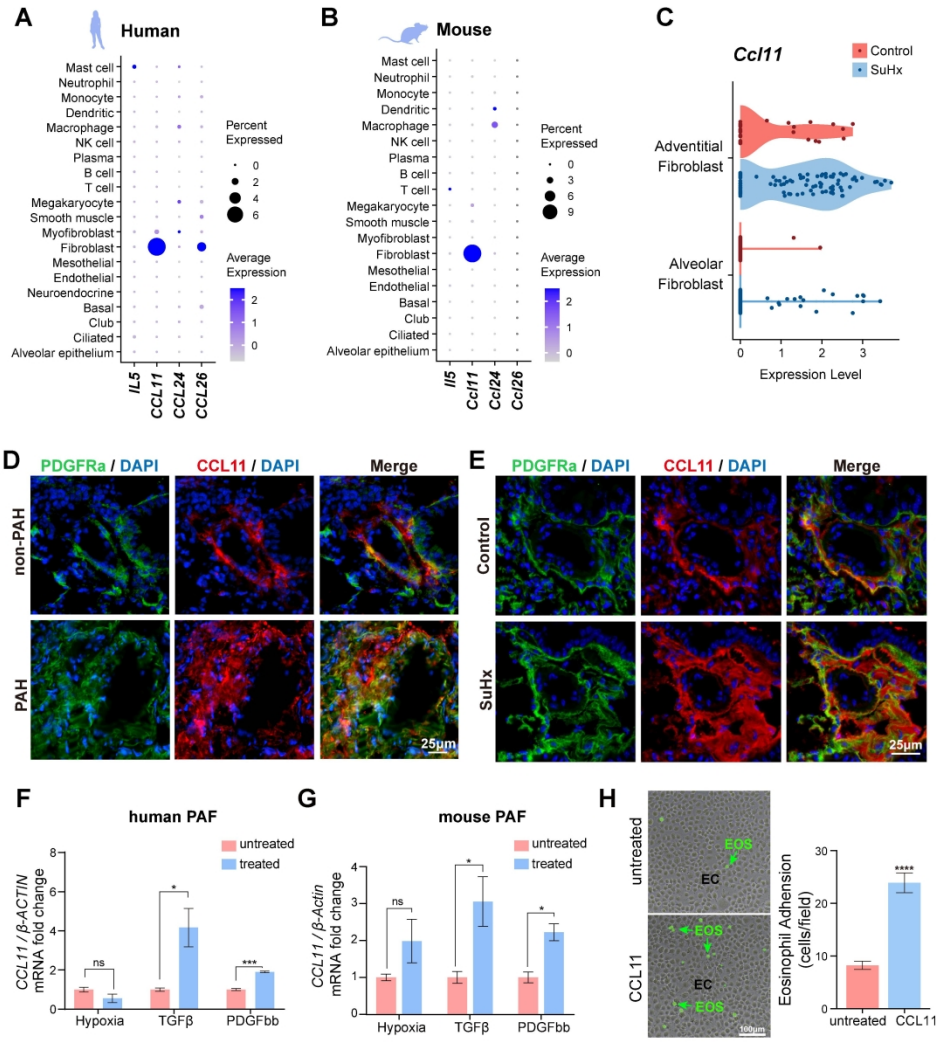

Figure 3. CCL11 expression in pulmonary adventitial fibroblasts.
A.Dot plots of gene expression (IL5, CCL11, CCL24, and CCL26) among cell clusters in human. B. Dot plots of gene expression (Il5, Ccl11, Ccl24, and Ccl26) among cell clusters in mouse. C. Violin plots of the expression of Ccl11 among two subgroups of fibroblasts in control and PH mice lung tissues. D. Representative images of CCL11 and PDGFRa immunofluorescent staining of the lung sections from control subjects (non-PAH) or PAH patients. Scale bar=25 μm. E. Representative images of CCL11 and PDGFRa immunofluorescent staining of the lung sections from control or PH mice. Scale bar=25 μm. F. Relative mRNA expression of CCL11 in human PAF under different treatments (n=3 for three independent repeats). G. Relative mRNA expression of Ccl11 in mouse PAF under different conditions (n=3 for three independent repeats). H. Representative images and quantification of EOS adhesive assay. Green arrow pointing at the 5-(and 6)-carboxyfluorescein diacetate succinimidyl ester (CFSE)-labeled EOS (green). Scale bar=100 μm. All data are shown as mean ± SEM. Differences were evaluated by unpaired two-tail Student's t-test. *P<0.05, ***P<0.001, ****P<0.0001, ns, no significance.

180x201mm (600 x 600 DPI)

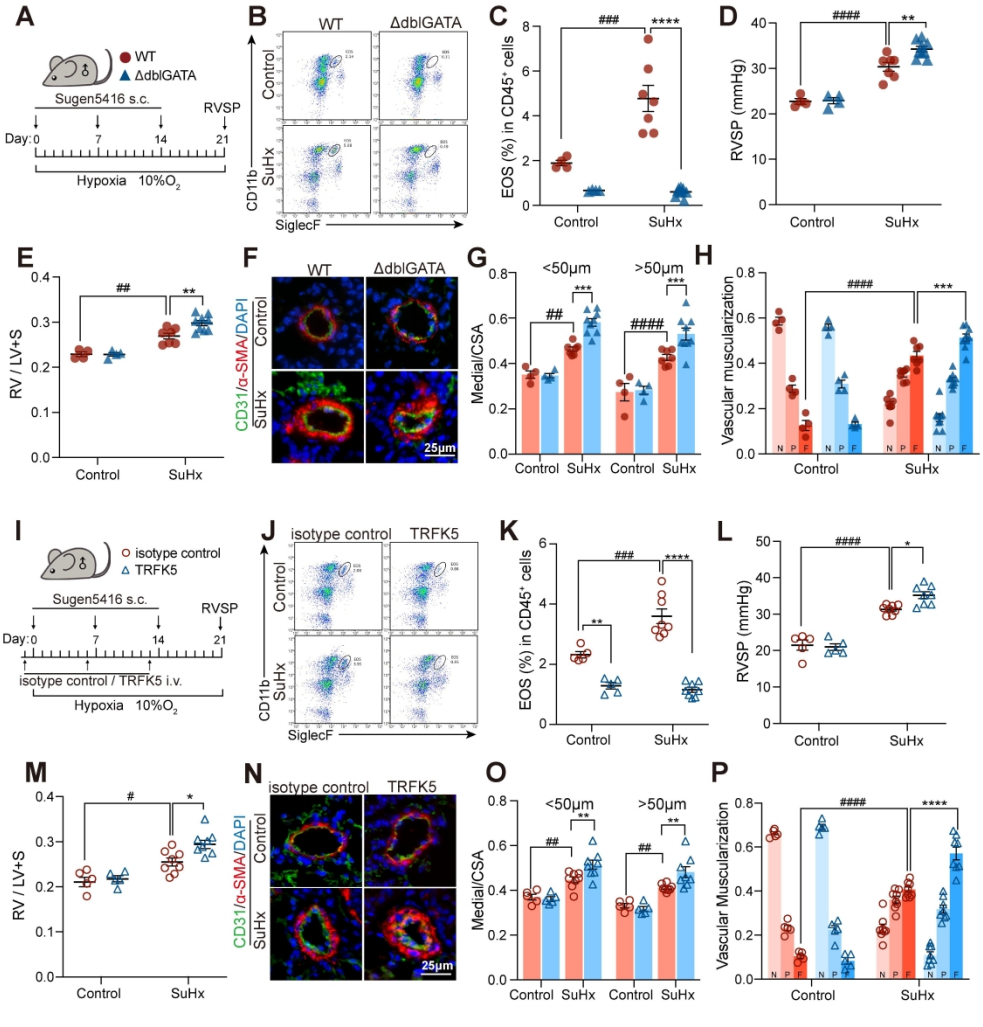

Figure 4. EOS deficiency and depletion exacerbate PH in mice.
A.Strategy for SuHx-induced PH in wildtype (WT) or EOS-deficient (ΔdblGATA) male mice (control: n=4 per group; SuHx: n=7 for WT, n=9 for ΔdblGATA). B. Representative flow cytometric analyses of CD11b+SiglecF+ EOS among CD45+ cells in lung tissues of WT or ΔdblGATA mice. C. The percentage of EOS among CD45+ cells in lung tissues of WT or ΔdblGATA mice. D. Right ventricular systolic pressure (RVSP) of WT and ΔdblGATA mice. E. RV/LV+S of the different experimental groups. F. Representative images of α-SMA and CD31 immunofluorescent staining of the lung sections from WT or ΔdblGATA mice. Scale bar=25 μm. G. Quantification of pulmonary vascular medial thickness to total cross sectional area (CSA), for vessels of 20-50 μm and 50-100 μm in diameter, respectively. H. Proportion of non-muscularized (N), partially muscularized (P), or full muscularized (F) pulmonary vessels of 20-100 μm in diameter. I. Strategy for SuHx-induced PH in male mice injected with isotype control antibody or TRFK5 (control: n=5 per group; SuHx: n=8 per group). J. Representative flow cytometric analyses of CD11b+SiglecF+ EOS among CD45+ cells in lung tissues of isotype control or TRFK5 treated mice. K. The percentage of EOS among CD45+ cells in lung tissues of isotype control or TRFK5 treated mice. L. RVSP of isotype control or TRFK5 treated mice. M. RV/LV+S of the different experimental groups. N. Representative images of α-SMA and CD31 immunofluorescent staining of the lung sections from isotype control or TRFK5 treated mice. Scale bar=25 μm. O. Quantification of wall thickness of the pulmonary vasculature, for vessels of 20-50 μm and 50-100 μm in diameter, respectively. P. Proportion of non-muscularized (N), partially muscularized (P), or full muscularized (F) pulmonary vessels of 20-100 μm in diameter. All data are shown as mean ± SEM. Differences between multiple groups were evaluated by two-way ANOVA with Bonferroni's post hoc test.

*P<0.05, **P<0.01, ***P<0.001 and ****P<0.0001 for ΔdblGATA versus WT mice, or TRFK5 versus isotype control-treated mice; #P<0.05, ##P<0.01,###P<0.001 ####P<0.0001 for mice in control versus SuHx groups.

180x185mm (600 x 600 DPI)

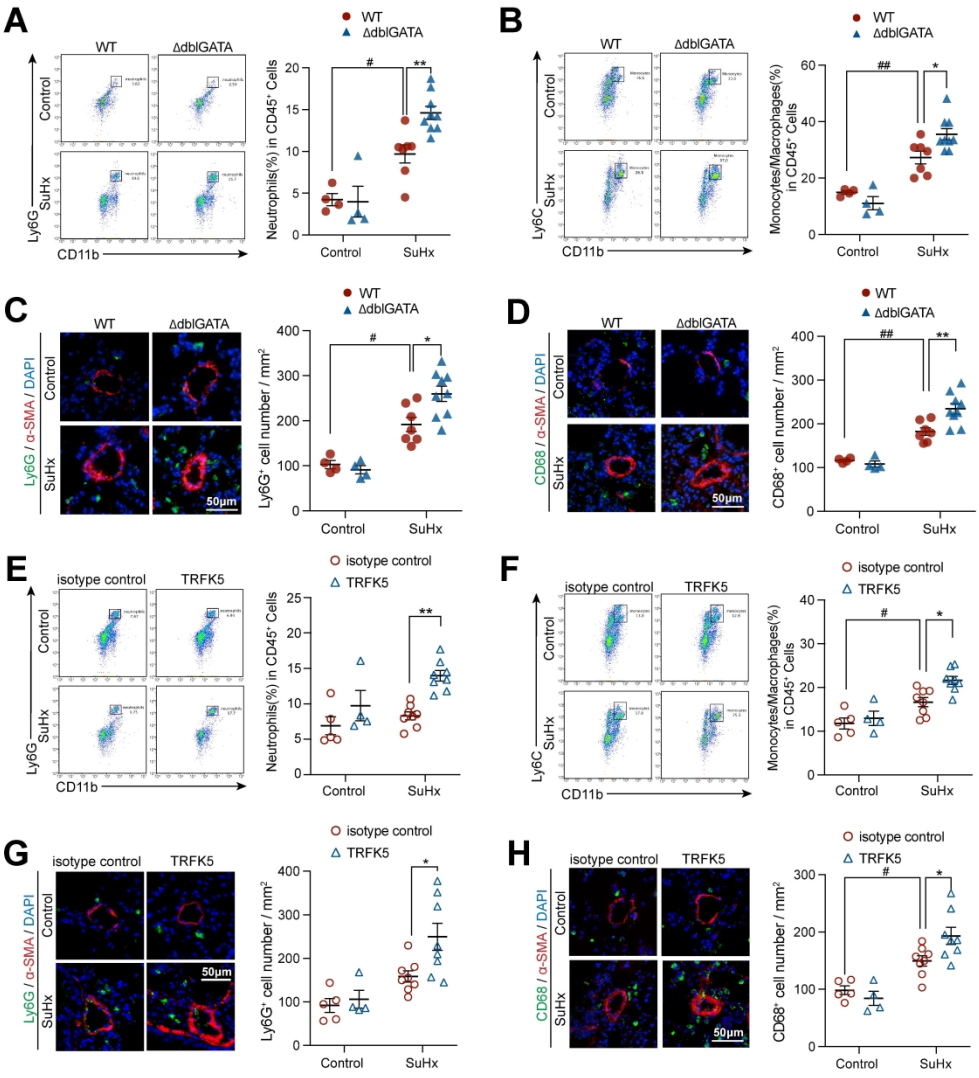

Figure 5. EOS deficiency or depletion promotes neutrophil and monocyte/macrophage accumulation in lung. A.Representative flow cytometric analyses of CD11b+Ly6G+ neutrophils among CD45+ cells in lung tissues of WT or ΔdblGATA male mice (left panel) and the percentage of neutrophils among CD45+ cells (right panel). B. Representative flow cytometric analyses of CD11b+Ly6C+ monocytes/macrophages among CD45+ cells in lung tissues of WT or ΔdblGATA male mice (left panel) and the percentage of monocytes/macrophages among CD45+ cells (right panel). C. Representative images of Ly6G and α-SMA immunofluorescent staining of lung sections from WT or ΔdblGATA male mice (left panel) and quantification of Ly6G+ cell numbers per mm2 lung tissue (right panel). Scale bar=50 μm. D. Representative images of CD68 and α-SMA immunofluorescent staining of lung sections from WT or ΔdblGATA male mice (left panel) and quantification of CD68+ cell numbers per mm2 lung tissue (right panel). Scale bar=50 μm. E. Representative flow cytometric analyses of CD11b+Ly6G+ neutrophils among CD45+ cells in lung tissues of isotype control or TRFK5 treated male mice (left panel) and the percentage of neutrophils among CD45+ cells (right panel). F. Representative flow cytometric analyses of CD11b+Ly6C+ monocytes/macrophages among CD45+ cells in lung tissues of isotype control or TRFK5 treated male mice (left panel) and the percentage of CD11b+Ly6C+monocytes/macrophages among CD45+ cells (right panel). G. Representative images of Ly6G and α-SMA immunofluorescent staining of lung sections from isotype control or TRFK5 treated male mice (left panel) and quantification of Ly6G+ cell numbers per mm2 lung tissue (right panel). Scale bar=50 μm. H. Representative images of CD68 and α-SMA immunofluorescent staining of lung

sections from isotype control or TRFK5 treated male mice (left panel) and quantification of CD68+ cell numbers per mm2 lung tissue (right panel). Scale bar=50 μm. Differences between multiple groups were evaluated by two-way ANOVA with Bonferroni's post hoc test. For A-D, control: n=4 per group; SuHx: n=7 for WT, n=9 for ΔdblGATA. For E-H, control: n=5 for isotype control, n=4 for TRFK5; SuHx: n=8 per group. All data are shown as mean ± SEM. *P<0.05, **P<0.01 and for ΔdblGATA versus WT mice, or TRFK5 versus isotype control-treated mice; #P<0.05 and ##P<0.01 for mice in control versus SuHx groups.

180x194mm (600 x 600 DPI)

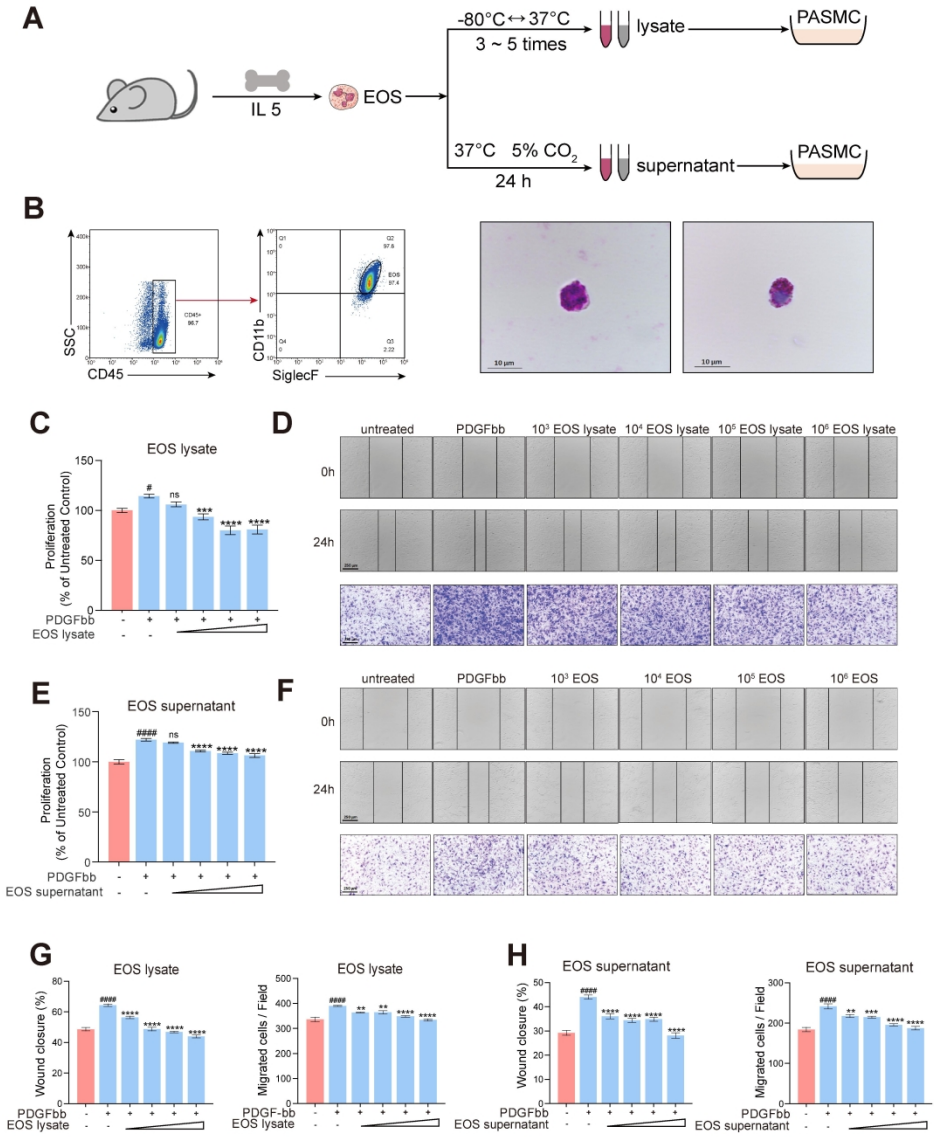

Figure 6. EOS abolishes PDGFbb-induced smooth muscle cell proliferation and migration. A.Strategy for in vitro experiments. B. Representative flow cytometric identification (left panel) and Wright-Giemsa staining (right panel) of liquid-cultured bone-marrow-derived EOS. Scale bar=10 μm. C. The percentage of mouse PASMC proliferation after treatment of PDGFbb (10 ng/mL) and different concentrations of EOS lysate (equivalent to 1×103, 1×104, 1×105, 1×106 EOS per mL) for 24 h compared with untreated control. D. Representative images of wound-healing (upper panel) and Boyden Chamber migration assay (down panel) for mouse PASMC after treatment of PDGFbb (10 ng/mL) and different concentrations of EOS lysate (equivalent to 1×103, 1×104, 1×105, 1×106 EOS per mL) for 24 h. Scale bar=250 μm. E. The percentage of mouse PASMC proliferation after treatment of PDGFbb (10 ng/mL) and different concentrations of EOS supernatant (equivalent to 1×103, 1×104, 1×105, 1×106 EOS per mL) for 24 h compared with untreated control, measured by CCK8. F. Representative images of wound-healing (upper panel) and Boyden Chamber migration assay (down panel) for mouse PASMC after treatment of PDGFbb (10 ng/mL) and different concentrations of EOS supernatant (equivalent to 1×103, 1×104, 1×105, 1×106 EOS per mL) for 24 h. Scale bar=250 μm. G. The percentage of wound closure (left panel) and

quantification of migrated PASMC (right panel) in D. H. The percentage of wound closure (left panel) and quantification of migrated PASMC (right panel) in F. All data are shown as mean ± SEM. Differences were evaluated by one-way ANOVA with Bonferroni's post hoc test. #P<0.05, ####P<0.0001 for PDGFbb-treated group compared with untreated-control group; **P<0.01, ***P<0.001, ****P<0.0001, ns, no significance for EOS-lysate/supernatant -treated groups versus PDGFbb-treated groups.

180x229mm (600 x 600 DPI)

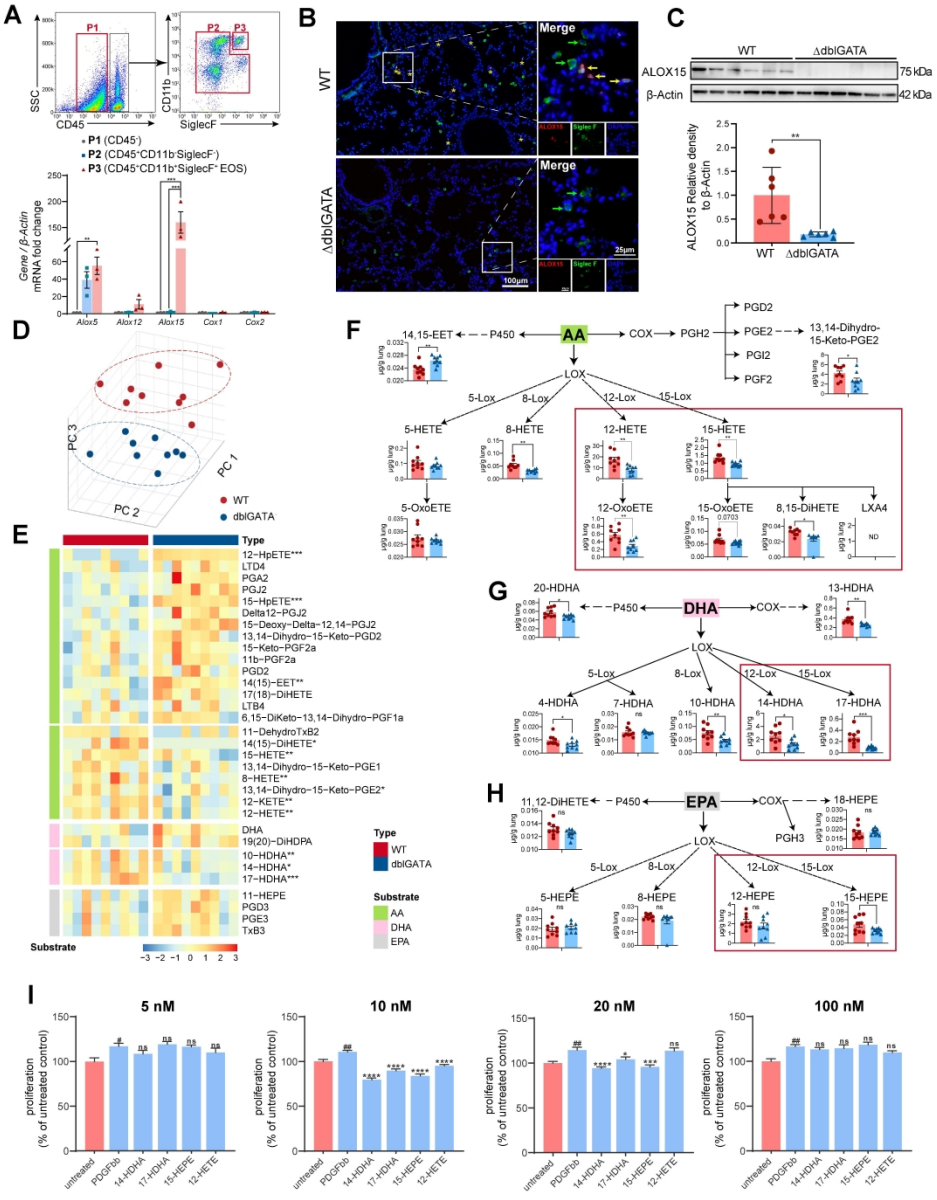

Figure 7. 12/15-lipoxygenase derivatives deficiency in lungs of ΔdblGATA mice.
Strategy for flow cytometric sorting from lung tissues of C57/BL6 mice (top panel) and relative mRNA expression of Alox5, Alox12, Alox15, Cox1 and Cox2 in sorted cells (bottom panel, n=3). B. Representative images of Alox15 and SiglecF immunofluorescent staining of lung sections from WT or ΔdblGATA mice. Scale bar=25 and 100 μm. C. Representative western blots (top panel) and quantification (bottom panel) of Alox15 in the lungs of WT and ΔdblGATA mice with PH(n=6 per group). D. Principal component analysis of lipidomics data. E. Heatmap showing key lipid derivatives differentially expressed in lung tissues of WT or ΔdblGATA mice with PH (n=9 per group). F. Quantification of Arachidonic acid (AA)-derived products in lung tissues of WT and ΔdblGATA mice with PH (n=9 per group). G. Quantification of Docosahexaenoic acid (DHA)-derived products in lung tissues of WT and ΔdblGATA mice with PH (n=9 per group). H. Quantification of Eicosapentaenoic acid (EPA)-derived products in lung tissues of WT and ΔdblGATA mice with PH (n=9 per group). I. The percentage of mouse PASMC proliferation after treatment of PDGFbb (10 ng/mL) and different concentrations of 12/15-LOX derivatives (5 nM, 10 nM, 20 nM, 100 nM) compared with untreated control, measured by CCK8. For A and I, differences between groups were evaluated by one-way

ANOVA with Bonferroni's post hoc test. For C, F-H, differences were evaluated by unpaired two-tailed Student's t-test. All data are shown as mean ± SEM. #P<0.05, ##P<0.01 for PDGFbb-treated group compared with untreated-control group, *P<0.05, **P<0.01, ***P<0.001,****P<0.0001 for 12/15-LOX derivatives-treated groups versus PDGFbb-treated groups, or WT versus ΔdblGATA mice with PH, ns, no significance, ND, not detected.

180x229mm (600 x 600 DPI)

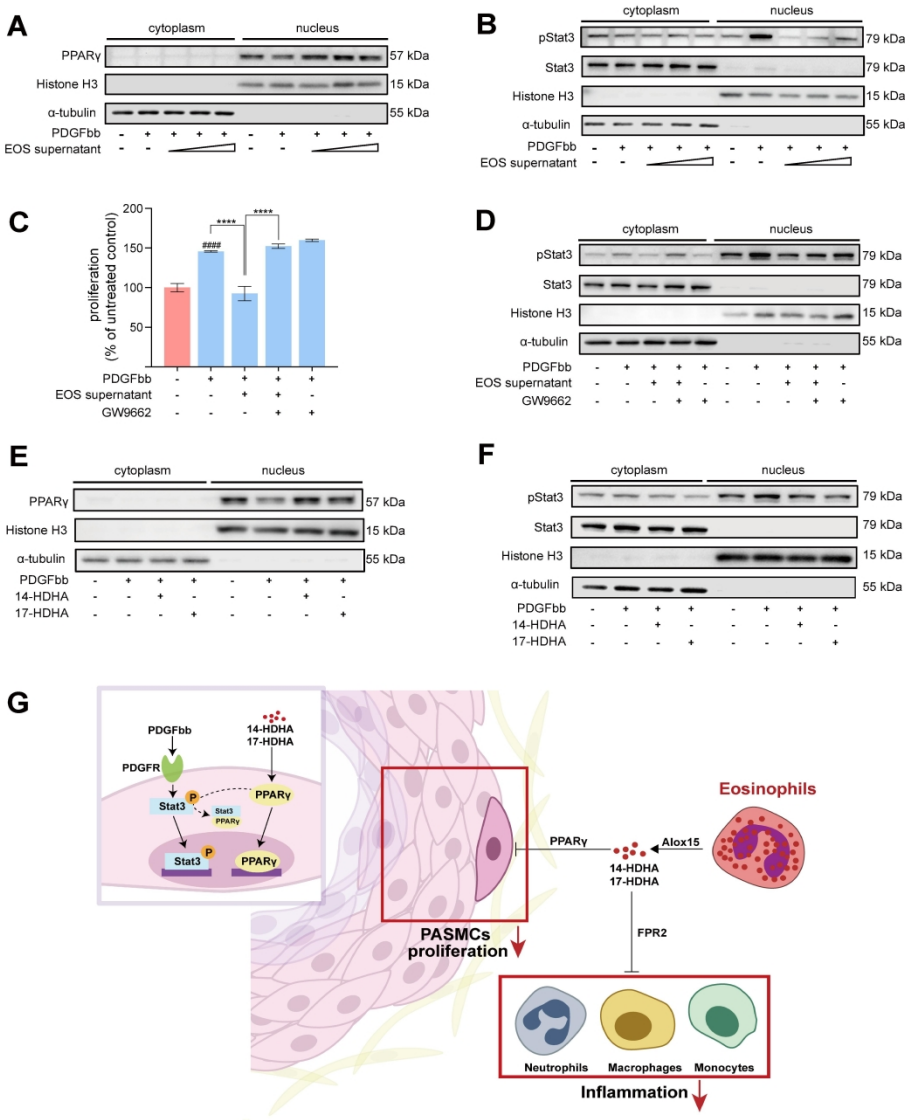

Figure 8. EOS-derived 14/17-HDHA inhibits PASMC proliferation via activating PPARγ. A.Representative western blots of PPARγ in cytoplasmic and nuclear extracts of mouse PASMC treated with PDGFbb and different concentrations of EOS supernatant (equivalent to 1×104, 1×105, 1×106 EOS per mL) for 24 h (n=3). B. Representative western blots of Stat3 and pStat3 in cytoplasmic and nuclear extracts of mouse PASMC treated with PDGFbb (10 ng/mL) and different concentrations of EOS supernatant (equivalent to 1×104, 1×105, 1×106 EOS per mL) for 24 h (n=3). C. The percentage of mouse PASMC proliferation pre-incubated with GW9662 (1 μM) or DMSO for 24 h, then treated with PDGFbb (10 ng/mL) and EOS supernatant (equivalent to 1×105 EOS per mL) for another 24 h compared with untreated control. D. Representative western blots of Stat3 and pStat3 in cytoplasmic and nuclear extracts of mouse PASMC pre-incubated with GW9662 or DMSO for 24 h, then treated with PDGFbb and EOS supernatant (equivalent to 1×105 EOS per mL) for another 24 h (n=3). E. Representative western blots of PPARγ in cytoplasmic and nuclear extracts of mouse PASMC treated with PDGFbb and 14-HDHA, 17-HDHA (10 nM) for 24 h (n=3). F. Representative western blots of Stat3 and pStat3 in cytoplasmic and nuclear extracts of mouse PASMC treated with PDGFbb and 14-HDHA, 17-HDHA (10 nM) for 24 h (n=3). G. Schematic representation of the

proposed mechanism underlying EOS-mediated protection in PH. For C, differences between groups were evaluated by one-way ANOVA with Bonferroni's post hoc test. ####P<0.0001 for PDGFbb-treated group compared with untreated-control group, ****P<0.0001 for other groups vs. EOS supernatant-treated groups.

180x229mm (600 x 600 DPI)

Eosinophils Protect Against Pulmonary Hypertension through 14-HDHA and 17-HDHA

Ting Shu, MD, PhD[1,†], Jiawei Zhang, PhD[1,†], Yitian Zhou, MD[1, 2], Zhihua Chen, PhD[3], Jinqiu Li, PhD[4], Qihao Tang, PhD[1], Wenqi Lei, PhD[1], Yanjiang Xing, PhD[4,*], Jing Wang, MD, PhD[1,*], Chen Wang, MD, PhD[1,4]

Supplementary Materials and Methods
Supplementary Table 1-2
Supplementary Figures and Legends 1-13

Supplementary Materials and Methods

Assessment of pulmonary hypertension

For hemodynamic characterization, at the end of experiments, mice were anesthetized with 2% pentobarbital (10 mg/kg) and right ventricular systolic pressure (RVSP) measurements were performed as previously described[1] using a closed chest technique. Briefly, a 22-gauge needle connected to pressure transducer interfaced with a PowerLab system (AD Instruments) was inserted into the right ventricle (RV) of anesthetized mouse through a xiphocostal angle approach, keeping the diaphragm intact without opening the chest. For rats, animals were anesthetized with 12% Urethane (10 mL/kg), and then the RVSP were measured by a PE catheter inserted into the right ventricle. The waveform was recorded and analysed using a PowerLab data-acquisition system (AD Instruments).

For right ventricle hypertrophy analysis, the free wall of the RV, left ventricle (LV) and septum (S) were then carefully dissected and individually weighed to calculate the Fulton index [ratio of RV/ (LV +S)] as a parameter of RV hypertrophy.

Flow cytometry and cell sorting

For lung total single cell suspension preparation, lungs were removed after infusing the pulmonary circulation with cold PBS. Lung tissues were minced into small pieces and treated by repeated rounds of enzymatic digestion and trituration with 200 U/mL collagenase I (Sigma Aldrich), 0.05 U/mL elastase (Sigma Aldrich), 5 U/mL neutral protease (Worthington), and 0.3 U/mL deoxyribonuclease I (Promega) according to a previously published protocol[2, 3].The digestion process lasted for 25 min at 37 °C. To measure B cells, $CD4^+$ and $CD8^+$ T cells, mast cells, dendritic cells (DCs), EOS, neutrophils and monocytes in lung tissue, single cell suspensions were stained with cell surface marker antibodies including PE-CD19 (115508, Biolegend), PE-CD3 (100205, Biolegend), FITC-CD4 (11-0041-82, Invitrogen), FITC-CD8a (11-0081-82, Invitrogen), PE-CD45 (103106, Biolegend), APC-CD117 (17-1171-82, Invitrogen), FITC-FcεRIα (11-5898-82, Invitrogen), FITC-CD45 (11-0451-85, Invitrogen), PE-CD11c (117308, Biolegend), APC-MHC-II (107614, Biolegend), PE-SiglecF (12-1702-82, Invitrogen), APC-CD11b (17-0112-82, Invitrogen), PE-Cyanine7-CD101 (25-1011-82, Invitrogen), FITC-CD11b (11-0112-85, Invitrogen), APC-Ly6G (127614, Biolegend), APC-Ly6C (128015, Biolegend) at

1:100 dilution ratio. Flow cytometry results were measured by Accuri C6 Plus Cytometer (BD Pharmingen) and analysed with FlowJo 7.6 software (FlowJo, LLC.). Cell sorting was performed on SONY SH900.

Assessment of EOS percentage in blood

Mouse EOS percentage in blood was assessed by flow cytometry. After red blood cell lysis, cells were labeled with CD45, CD11b, SiglecF, and assessed by Accuri C6 Plus Cytometer, BD Pharmingen. For rat and human blood samples, the percentages of EOS were measured by ADVIA 2120, Siemens and XN2000, Sysmex respectively.

Histological analyses

For paraffin sections, as soon as being removed, lung tissues from PAH patients and non-PAH donors were fixed in 10% formaldehyde at 4 °C for 24 h and embedded in paraffin. For frozen sections, after hemodynamic measurements, the perfused left lungs of mice were first fixed in 4% paraformaldehyde (PFA) for 2 h, tissues were then equilibrated in 30% sucrose for 72 h at 4 °C and embedded in optimal cutting temperature compound (OCT; 4583, SAKURA). The fixed lung tissues were randomly cut into serial parallel sections and embedded in OCT in the same orientation. To perform morphometric analyses, the slides were sectioned in 5-μm thickness.

For H&E staining, the slices were stained with hematoxylin and eosin according to the manufacturer's instructions (Zhong Shan Jin Qiao).

For Wright-Giemsa staining, the smears were stained according to the manufacturer's instructions (BASO Diagnostics inc.).

For Masson's trichrome staining, the slices were stained according to the manufacturer's instructions (Servicebio).

For immunohistochemistry and immunofluorescence staining, the slides were incubated with the appropriate primary antibody at 4 °C overnight followed by an Alexa Fluor 488- or 594- (Thermo, 1:1000, 45 min) or horseradish peroxidase (HRP)-conjugated secondary antibody (Zhong Shan Jin Qiao). Five-color immunofluorescence staining was performed according to the PANO 5-plex IHC kit (0080100100, PANOVUE). Primary antibodies against α-SMA (ab5694, 1:400), CD68 (ab53444, 1:200), Ly6G (ab25377, 1:200), Histone H3(citrulline R2+R8+R17;

ab281584, 1:200), 15-Lipoxygenase 1 (ab244205, 1:200), CD31 (ab182981, 1:200) were obtained from Abcam. Primary antibody against SiglecF (552125, 1:200) and CD31 (550274, 1:100) were obtained from BD Pharmingen. Primary antibodies against PDGFRα (60045-1-1g, 1:200), CC10 (10490-1-AP, 1:200) was obtained from Proteintech and antibody against ECP (A1854, 1:100) were obtained from Abclonal. Primary antibodies against CCL11 (sc-373767, 1:200) and Vimentin (sc-6260,1:200) was obtained from Santa Cruz. Primary antibody against α-SMA (A5228, 1:400) was obtained from Sigma-Aldrich.

For the assessment of the wall thickness in experimental PH models, 9 fields from 3 lung sections per animal were randomly selected and captured. All images taken from the lung sections were coded so that the experimenters were blinded during assessment. Small vessels (<100 μm in diameter) were selected from those accompanied respiratory bronchioles or more distal airways. Approximately 20-40 small vessels were selected and categorized into two groups (20-50 μm and 50-100 μm in diameter). The wall thickness of each group was calculated respectively with the formula, [medial wall area/ total vessel area) × 100]%, as previously described [4].

For the assessment of small pulmonary vessel muscularization (under 100 μm in diameter), the extent of circumferential α-SMA-positive staining was categorized as nonmuscularization (N), partial muscularization (P) and full muscularization (F), as previously described. Briefly, full muscularization (F) was defined as a distinct α-SMA-positive staining throughout the vessel cross section (positive in double elastic lamina). Partial muscularization (P) was considered when at least half of the circumference of vessels showed α-SMA-positive[5]. Less than half of the vascular circumference showed positive staining was considered as nonmuscularization (N). 30-50 randomly selected vessels (accompanied respiratory bronchioles or more distal airways) from 9 fields taken from 3 lung sections per animal (as described above) were assessed by experimenters who were blinded to the experiments. Frequency for each type of muscularization from each animal was presented as a ratio to total number of vessels counted.

For the assessment of the vascular fibrosis in experimental PH models, 9 fields from 3 lung sections per mouse were randomly selected and captured. The fibrosis area of each field was quantitatively analysed by the computer program ImagePro.

All the assessments and analyses were completed by experimenters blinded to the

experiments.

Lung lipidomic analyses

Lung tissue samples of SuHx EOS-deficient KO mice and WT control mice were harvested and processed for UHPLC-MS/MS, and the quantification was based on calibration curves. All oxylipins (oxidized fatty acids) and deuterated standards as internal standards were purchased from Cayman Chemical. Methanol (LC-MS grade), acetonitrile, isopropanol, acetic acid and formic acid were the products of Fisher Scientific. SPE columns (Strata-X) were bought from Phenomenex. Other materials were obtained from Shanghai Anpel Laboratory Technologies. The quality control (QC) sample was obtained by isometrically pooling all the prepared samples. The concentrations (*C*, μg/mL) of oxidized fatty acid in prepared sample (for determination) were quantified automatically, and finally output for quantitative calculation of each gram lung tissue samples of mouse in Excel with the following formula,

Content (μg/g sample) $=C \times V/m$

where *C* is the concentration quantified in prepared sample (μg/mL), *V* is the volume of reconstituted solvent (μL), *m* is the weight of tissue sample (mg).

Sample preparation and metabolic profiling were performed with standard procedures in cooperation with Phenions Biotech (Suzhou, China).

Single-cell RNA-seq and analyses

Lung tissues from control or SuHx mice were harvested and scRNA-seq were performed. The lung tissue was digested as described in flow cytometry. The digested tissues were neutralized with DMEM containing 10% FBS (Gibco) and filtered through a 40-μm cell strainer (Invitrogen) to obtain single-cell suspensions. Live lung cells were sorted in PBS containing 0.5% BSA using a 100-μm nozzle on a Moflo-XDP cell sorter (Beckman). Single-cell suspensions of both groups were loaded on a Chromium Single-Cell Controller (10X Genomics) to generate single-cell and gel bead emulsion (GEM). The single-cell sequencing library was prepared according to the instructions of the Chromium Single-Cell 3’ Library & Gel Bead Kit

v2 (10X Genomics). The libraries were sequenced on an Illumina HiSeq X Ten in paired-end reads to enable approximately 50,000 reads per single-cell (Novo Generation Bioinformatics Technology Co., Ltd.).

The 10X Genomics single-cell transcriptome sequencing data were filtered and aligned to the GRCm38 (mm10) mouse reference genome using the Cell Ranger software suite version 5.0 pipeline[6]. For further analyses and statistics, based on the barcode and gene expression matrix, single-cell data were quality controlled, log-normalized and scaled by the R package Seurat version 3.2[7, 8] with the following parameters: unique gene counts per cell >200, reads per cell >300, and percentage of mitochondrial genes <15%.

Human lung cell atlas[9] with accession EGAS00001004344 was hired in further cell annotation analysis. Canonical correlation analysis (CCA) was performed to integrate mouse and human scRNA-seq data based on homologous genes between the two species and eliminate batch effect.

The integrated data assay was hired for the further analysis, including liner dimension reduction: principal component analysis (PCA) and nonlinear dimension reduction: uniform manifold approximation and projection (UMAP). Unsupervised cluster detection algorithms were performed stepwise based on integrated data assay, during which the top 50 significant PCA dimensions were considered and resolution for cluster identification was set as 2. Annotation of each cell from human lung cell atlas were inherited, combined with markers of each cell types were considered as annotation to each cell cluster.

Cell culture

For mouse EOS culture, EOS were isolated and cultured as previously reported[10]. In brief, bone marrow cells were collected from mouse femurs and tibias, centrifuged for 10 min at 1000 rpm, followed by lysing red blood cells. Once red blood cells were lysed, the cells were suspended in 10 mL of PBS prior to cell counting. Cells with a concentration of 10^6 cells/mL were plated in a T75 flask and cultured in a basal medium containing mouse stem cell factor (SCF; 100 ng/mL, 250-03, PeproTech) and mouse Flt-3-ligand (FLT3-L; 100 ng/mL, 250-31L, PeproTech) for 4 days. On day 4, culture media were replaced with the same basal medium containing recombinant mouse IL 5 (10 ng/mL, 215-15, PeproTech), without SCF or FLT3-L. Half of the

culture media were changed with fresh media containing IL 5 every other day until the Day 14.

For primary mouse endothelial cell culture, primary pulmonary endothelial cells were isolated as previously reported[11]. In brief, lung tissue single-cell suspensions were obtained as described in flow cytometry. Cell suspensions were incubated with CD31 microbeads (130-097-418, Miltenyi Biotec) for 15 min on ice. Then LS columns (130-042-401, Miltenyi Biotec) were used to collect endothelial cells positively labeled by CD31 microbeads via magnetic separation according to the manufacturer's instructions. The isolated primary endothelial cells were cultured in endothelial cell medium (ECM; Sciencell).

Primary mouse and human pulmonary arterial fibroblasts (PAFs) were purchased from Procell (CP-M012 for mouse PAFs; CP-H006 for human PAFs) and cultured in fibroblast culture medium (Procell, CM-M012 for mouse PAFs; CM-H006 for human PAFs). Mouse PAECs and PASMCs were purchased from Sciencell, cultured in ECM (Sciencell) and smooth muscle cell medium (SMCM; Sciencell), respectively. All cells were maintained in a sterile, humidified cell culture incubator at 37 ℃ with 5% CO_2. After reaching confluence, cells were passaged by using 0.05% trypsin-EDTA. 3-8 passage cells equilibrated in serum-free medium for 24 h were used for all experiments.

Cell stimulations

Cells were serum-starved for 24 h and then pre-incubated and stimulated as described in the figure legends, with a single or combination of the following stimulations (unless specified differently in the figure legends).

For mouse PASMCs, after 24 h of starvation, the cells were incubated with PDGFbb (10 ng/mL, 315-18, PeproTech), then with different concentrations of EOS lysates or supernatants (10^3, 10^4, 10^5, 10^6 cells/mL) for 24 h. GW9662 (M6191; Sigma-Aldrich) was used at 1 μM. Lipid derivatives 17-HDHA (33650), 14-HDHA (33550), 12-HETE (34550) and 15-HEPE (32700) were purchased from Cayman and administrated at 5, 10, 20, 100 nM in an assay-dependent way.

For mouse neutrophils and monocytes, after 24 h of starvation, the cells were incubated with 14-HDHA (10 nM) or 17-HDHA (10 nM) for 30 min. WRW4 (878557-55-2, MCE) were used at 10 μM.

For mouse and human PAFs, after 24 h of starvation, the cells were incubated under

hypoxic condition, or incubated either with PDGFbb (10 ng/mL, 315-18; 100-14B, PeproTech), or TGF-β1 (10 ng/mL, 7666-MB-005/CF, R&D Systems; 100-21, PeproTech) for 24 h.

Cell adhesion and transmigration assay

For eosinophil adhesion assay, primary pulmonary endothelial cells were planted and cultured on 6-well plates to reach a density of over 80%. The primary endothelial cells were then co-cultured with 5×10^5 EOS /mL, with or without the stimulation of CCL11 (1 μg/mL, 250-01, PeproTech). EOS was labelled with 5(6)-Carboxyfluorescein diacetate succinimidyl ester (CFSE) according to the manufacturer's instructions (HY-D0938, MCE). After 30 min, culture medium and unattached cells were removed by washing endothelial cell monolayers with PBS twice. The numbers of CFSE-tracked EOS were counted manually in 9 randomly chosen fields using a microscope (DS-Pi2, Nikon).

For neutrophil/monocyte adhesion assay, neutrophils and monocytes were isolated from mouse bone marrow or peripheral blood using discontinuous Percoll gradients (P9201 and P5230, Solarbio) according to the manufacturer's instructions. 96-well plates were coated with mouse ICAM-1–Fc (2 μg/mL, 796-IC-050, R&D Systems) and blocked with 1% BSA for 1 h. Cells were then immediately plated and incubated at 37 °C for 10 min. Nonadherent cells were removed by PBS washing. The bound cells were stained with 0.4% crystal violet, lysed in 0.5% Triton X-100. The absorbance was measured at 595 nm.

For neutrophil/monocyte transmigration assays, 5-μm-pore polycarbonate filters (3421, Corning) were coated with ICAM-1–Fc (2 μg/ml) and placed in 24-well plates filled with culture medium containing CXCL1 (1 μg/mL, 250-11, PeproTech) or CCL2 (1 μg/mL, 250-10, PeproTech). Cells were placed in the upper chamber followed by incubation for 1 h at 37 °C, then cells in the lower chamber were collected and counted using CountessII (Invitrogen).

Cell proliferation assay

The growth of PASMCs was measured using a Cell Counting Kit-8 (CCK8; Dojindo) according to the manufacturer's protocol. Briefly, after 24 h of starvation, 5×10^3 cells were seeded in 96-well plates for different treatments. After 24 h, fresh culture medium containing 10 μL CCK8 solution was added, and the plate was incubated for

1.5 h at 37 °C. The absorbance was measured at 450 nm and 570 nm.

Cell migration assay

For wound-healing assay, the assay was performed as previously described[6]. Briefly, PASMCs were planted and cultured on 6-well plates to reach a density of over 90%, the monolayer was scratched with a P200 pipette tip, and the edge was labeled with a traced line. After injury, the ablated cells were gently washed away with PBS. PASMC migration from the edge of the injury site was quantified by measuring the area between the wound edges before (wound area A_0) and after recovery (healing area A_{24}) using light microscopy and the computer program ImageJ. The wound closure area was calculated as follows: (migration area (%) = $(A_0 – A_{24})/A_0 \times 100$).

For Boyden chamber migration assay, an 8-μm-pore polycarbonate filter (3422, Corning) was used. The PASMCs were seeded at a density of 3×10^4 cells per well in the upper chamber of the transwell chambers in 24-well plates, and different stimulation medium was added to the lower chamber. After 24 hours, the upper surface of the membrane was washed with PBS and swabbed mildly with a cotton bud to remove nonmigrated cells. The migrated cells on the lower surface were fixed in 4% paraformaldehyde and stained with 0.4% crystal violet. The numbers of migrated cells per well were counted manually in 5 randomly chosen fields using a microscope (DS-Pi2, Nikon).

ELISA

Mouse serum IgE (88-50460-88, eBioscience), IgA (70-EK274-96, MultiSciences Biotech), IgG (70-EK271-96, MultiSciences Biotech) were measured according to the manufacturer’s instructions. Lung tissue IL5 (RK00037, Abclonal) and CCL11 (70-EK2130/2-96, MultiSciences Biotech) levels were measured from tissue lysis.

RT-qPCR

Total RNA was extracted from the frozen lung tissues or cultured cells by TRIzol reagent (Invitrogen) according to the manufacturer’s instructions. The concentration and purity of the RNA samples were evaluated with Nanodrop. Reverse-transcription of the first chain was performed using a FastKing RT kit (Tiangen Biotech) according to the manufacturer’s protocols. The mRNA expression levels of genes were

examined by RT-qPCR. The expression of each gene in this study was normalized to that of the reference gene. The primer sequences are shown in **Supplementary Table 2**.

Western blot analyses

Cell lysates or tissue pieces were prepared by adding the lysis buffer supplemented with phosphatase inhibitor cocktail PhosphoSTOP EASYpack (04906845001, Roche). Nuclear/cytoplasmic extracts were acquired by using a Nuclear and Cytoplasmic Protein Extraction Kit (P0027, Beyotime) according to the manufacturer's instructions. Protein samples (20 μg) were fractionated by sodium dodecyl sulfate-polyacrylamide gel electrophoresis (SDS-PAGE) using 12-15% polyacrylamide gels. Separated protein was transferred to a 0.45 μm PVDF membrane. After blocking in 5% milk/Tris-buffered saline-Tween (TBST) for 1 h at room temperature, the membrane was incubated with the appropriate primary antibody: β-ACTIN (AC026, Abclonal), α-TUBULIN (T6074, Sigma Aldrich), Histone H3 (17168-1-AP, Proteintech), Collagen I (ab254113, Abcam), 15-Lipoxygenase 1 (ab244205, Abcam), PhosphoStat3 (9131, Cell Signaling Technology), Stat3 (9139, Cell Signaling Technology), PhosphoSmad3 (9520, Cell Signaling Technology), Smad3 (9523, Cell Signaling Technology), PPARγ (2435, Cell Signaling Technology) at 4°C overnight. After washing three times with TBST, the membrane was incubated with corresponding HRP-labeled rabbit or mouse secondary antibodies (Invitrogen, 1:5,000 or 1:10,000). Immunoreactive bands were visualized with Super Signal West Pico Chemiluminescent Substrate (Pierce).

Statistical analyses

All statistical analyses were performed using GraphPad Prism 9.0. Data are presented as mean ± standard error of mean (SEM). F test were used for equality of variances. For equal variances, parametric tests were used. An unpaired two-tailed Student's *t*-test was performed to compare the differences between two groups. A one-way ANOVA with the Bonferroni's post hoc test or two-way ANOVA with Bonferroni's post hoc test was performed to evaluate differences between multiple groups. A *P*-value <0.05 was considered statistically significant. Randomization and blinded

analyses were used whenever possible.

Supplementary Table

Supplementary Table 1. Demographic and clinical characteristics of PAH patients and healthy people.

Feature	Patients with PAH (N=123)	Control Subject (N=119)
Age at sampling, y	31.9 ± 8.1	33.5 ± 5.1
Female: Male(ratio)	3.1:1	2.8:1
NYHA functional class		N/A
I	5/123	
II	50/123	
III	62/123	
IV	6/123	
Comorbid conditions		N/A
Tricuspid regurgitation	8/123	
Arrhythmia	9/123	
Hypertension	14/123	
Hypothyroidism	5/123	
Hypohepatia	15/123	
Hyperuricemia	8/123	
Hyperlipidemia	4/123	
Hyperglycemia	2/123	
Sleep apnea syndrome	8/123	
Hemodynamics		N/A
Mean right atrial pressure, mmHg	5.3±4.2	
Pulmonary capillary wedge pressure, mmHg	7.0±3.6	
Mean pulmonary artery pressure, mmHg	55.8±15.6	
Cardiac index	2.9±1.0	
Cardiac output, L/min	4.7±1.6	
Total Pulmonary Resistance, dyn·s·cm-5	1114.7±534.4	
6-min walk distance, m	424.4±98.3	N/A
SvO_2%	68.0±7.8	N/A
NT-proBNP, pg/mL	1212.0±1153.8	N/A
Creatinine, μmol/L	74.5±15.8	N/A
Uric Acid, μmol/L	427.4±136.5	N/A
C Reactive Protein, mg/L	2.89±2.7	N/A
PAH therapy		N/A
Prostacyclin analogue	6/123	
Endothelin antagonist	28/123	
Phosphodiesterase5 inhibitor	84/123	

Values are presented by mean ± SD. NYHA, New York Heart Association; SvO_2, Oxygen saturation of mixed venous blood; NT-proBNP, N-terminal pro brain natriuretic peptide. Differences between groups were assessed by unpaired two-tailed *t*-test.

Supplementary Table 2. Sequences of qPCR primers.

Name		Sequence
Il5 (mouse)	Forward	5' AGCAATGAGACGATGAGGCT 3'
	Reverse	5' GTACCCCCACGGACAGTTTG 3'
Ccl11 (mouse)	Forward	5' TCCATCCCAACTTCCTGCTGCT 3'
	Reverse	5' CTCTTTGCCCAACCTGGTCTTG 3'
Ccl24 (mouse)	Forward	5' CGTGTTGCATCTTCCCCATAGATTC 3'
	Reverse	5' GCAGCCTGGTAAAGCGTCAATA 3'
Ccl26 (mouse)	Forward	5' TCGCTATGTCCTGCTGCCCTAA 3'
	Reverse	5' CTGGACACAGAATTGCTTACCTG 3'
IL5 (human)	Forward	5'TGCTGATAGCCAATGAGACTCTG 3'
	Reverse	5' ACCCCCTTGCACAGTTTGAC 3'
CCL11 (human)	Forward	5' GCTACAGGAGAATCACCAGTGG 3'
	Reverse	5' GGAATCCTGCACCCACTTCTTC 3'
CCL24 (human)	Forward	5' TGAGAACCGAGTGGTCAGCTAC 3'
	Reverse	5' TTCTGCTTGGCGTCCAGGTTCT 3'
CCL26 (human)	Forward	5' GGGAGTGACATATCCAAGACCTG 3'
	Reverse	5' CAGACTTTCTTGCCTCTTTTGGTA 3'
Alox5 (mouse)	Forward	5' TCTTCCTGGCACGACTTTGCTG 3'
	Reverse	5' GCAGCCATTCAGGAACTGGTAG 3'
Alox12 (mouse)	Forward	5' CTCTTGTCATGCTGAGGATGGAC 3'
	Reverse	5' AAGAGCCAGGCAAGTGGAGGAT 3'
Alox15 (mouse)	Forward	5' GGCTCCAACAACGAGGTCTAC 3'
	Reverse	5' AGGTATTCTGACACATCCACCTT 3'
Cox1 (mouse)	Forward	5' GAATGCCACCTTCATCCGAGAAG 3'
	Reverse	5' GCTCACATTGGAGAAGGACTCC 3'
Cox2 (mouse)	Forward	5' GCGACATACTCAAGCAGGAGCA 3'
	Reverse	5' AGTGGTAACCGCTCAGGTGTTG 3'

Supplementary Figures and Legends

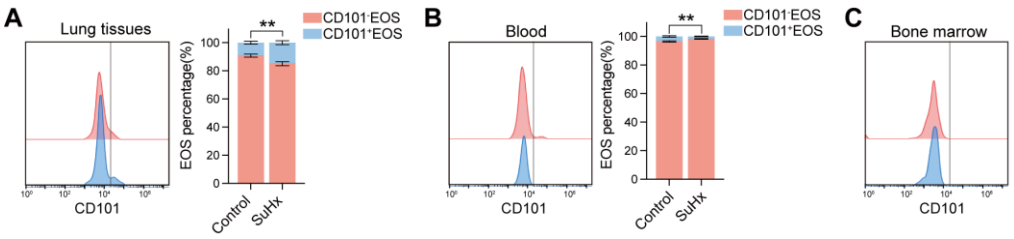

Supplementary Figure 1. Percentage of CD101$^-$ EOS subgroups in PH mice.

A. Flow cytometric analyses of CD101$^-$/CD101$^+$ subgroups among EOS in lung tissues of control or PH mice (n=8 per group). **B.** Flow cytometric analyses of CD101$^-$/CD101$^+$ subgroups among EOS in peripheral blood of control or PH mice (n=8 per group). **C.** Representative flow cytometric analyses of CD101$^-$/CD101$^+$ subgroups among EOS in bone marrow of control or PH mice (n=8 per group). All data are shown as mean ± SEM. For A and B, differences were analysed by unpaired two-tailed Student's *t*-test. ***P* <0.01.

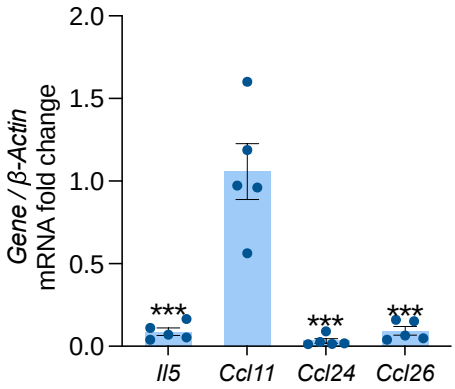

Supplementary Figure 2. Relative *Il5, Ccl11, Ccl24, Ccl26* expression in lungs. Relative mRNA expression of *Il5, Ccl11, Ccl24, Ccl26* in mouse lungs (n=5). All data are shown as mean ± SEM. Differences between groups were evaluated by unpaired two-tailed Student's *t* test. ****P* <0.001, compared with *Ccl11*.

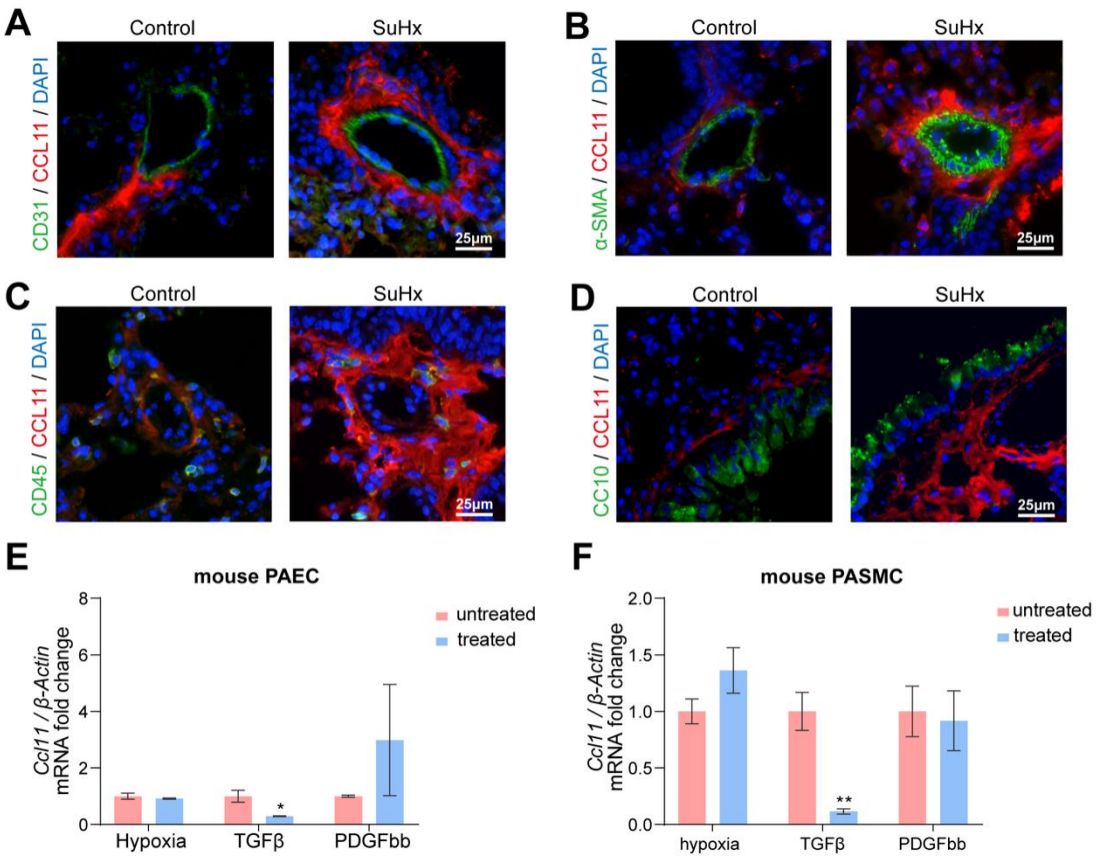

Supplementary Figure 3. CCL11 expression in other cell types in mice.

A. Representative images of CCL11 and CD31 immunofluorescent staining of the lung sections from control or PH mice. **B.** Representative images of CCL11 and α-SMA immunofluorescent staining of the lung sections from control or PH mice. **C.** Representative images of CCL11 and CD45 immunofluorescent staining of the lung sections from control or PH mice. **D.** Representative images of CCL11 and CC10 immunofluorescent staining of the lung sections from control or PH mice. **E.** Relative mRNA expression of *Ccl11* in mouse PAEC under different conditions (n=3 per group). **F.** Relative mRNA expression of *Ccl11* in mouse PASMC under different conditions (n=3 per group). All data are shown as mean ± SEM. Differences between groups were evaluated by unpaired two-tailed Student's *t* test. **P* <0.05, ***P* <0.01, compared with untreated groups. Scale bar=25 μm.

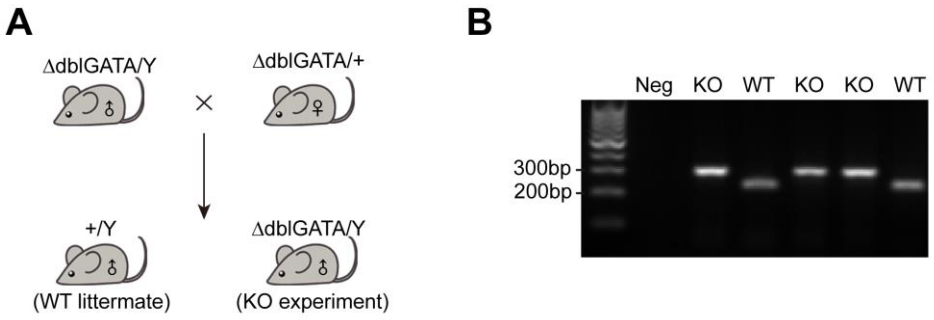

Supplementary Figure 4. Breeding strategy of EOS-deficient ΔdblGATA mice.

A. Schematic diagram of breeding strategy of ΔdblGATA mice. **B.** Representative image of ΔdblGATA mice genotype identification by PCR.

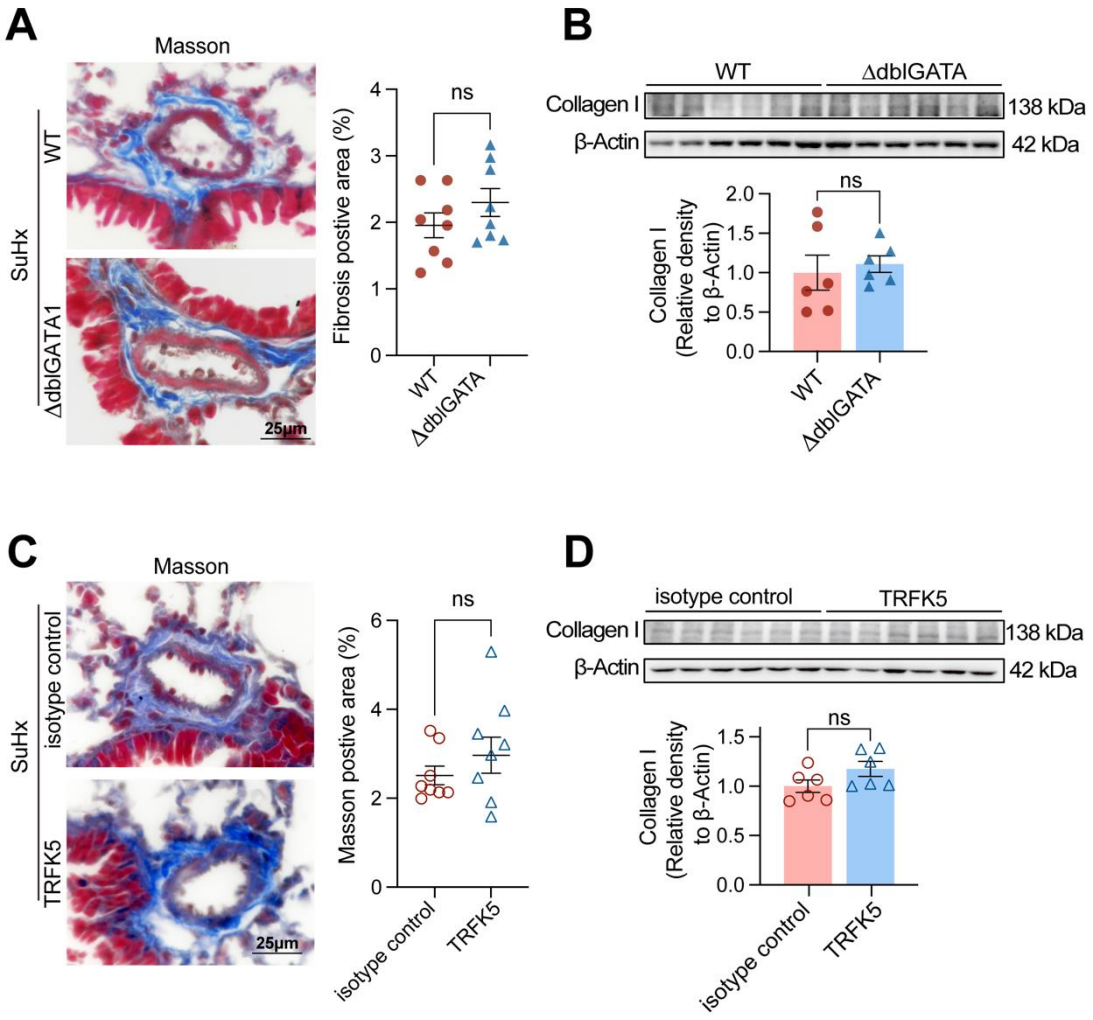

Supplementary Figure 5. Vascular collagen deposition of EOS-deficient/depleted PH mice.

A. Representative images and quantification of Masson's trichrome staining of the lung sections from WT or ΔdblGATA mice (n=8 per group). **B.** Representative western blots (top panel) and quantification (bottom panel) of Collagen I in the lungs of WT and ΔdblGATA mice with PH (n=6 per group). **C.** Representative images and quantification of Masson's trichrome staining of the lung sections from isotype control or TRFK5 treated PH mice (n=8 per group). **D.** Representative western blots (top panel) and quantification (bottom panel) of Collagen I in the lungs of isotype control or TRFK5 treated mice with PH (n=6 per group). All data are shown as mean ± SEM. Differences between groups were evaluated by unpaired two-tailed Student's *t* test. ns for no significance.

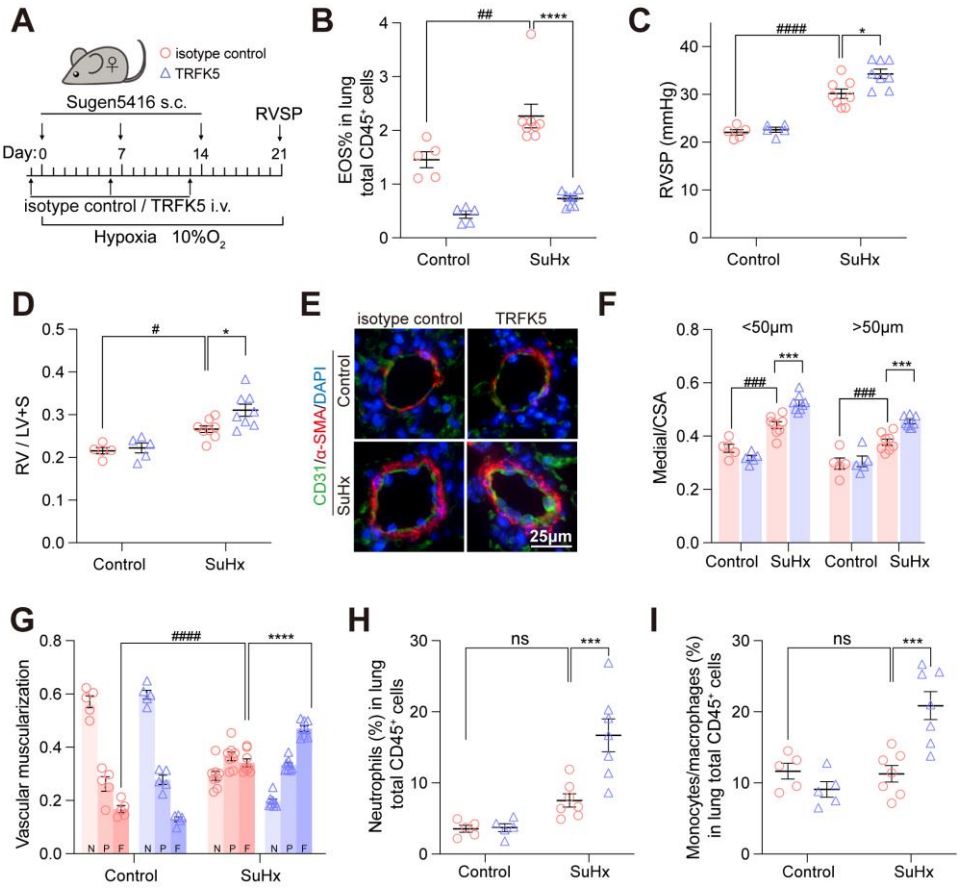

Supplementary Figure 6. EOS depletion exacerbated PH in female mice.

A. Strategy for SuHx-induced PH in female mice injected with isotype control antibody or TRFK5 (control: n=5 per group; SuHx: n=8 per group). **B.** The percentage of EOS among $CD45^+$ cells in lung tissues of isotype control or TRFK5 treated female mice. **C.** RVSP of isotype control or TRFK5 treated female mice. **D.** RV/LV+S of the different experimental groups. **E.** Representative images of α-SMA and CD31 immunofluorescent staining of the lung sections from isotype control or TRFK5 treated mice. Scale bar=25 μm. **F.** Quantification of wall thickness of the pulmonary vasculature, for vessels of 20-50 μm and 50-100 μm in diameter, respectively. **G.** Proportion of non-muscularized (N), partially muscularized (P), or full muscularized (F) pulmonary vessels of 20-100 μm in diameter. **H.** The percentage of neutrophils among $CD45^+$ cells. **I.** The percentage of monocytes/macrophages among $CD45^+$ cells. All data are shown as mean ± SEM. Differences between multiple groups were evaluated by two-way ANOVA with Bonferroni's post hoc test. *P<0.05, ***P<0.001 and ****P<0.0001 for TRFK5 versus isotype control-treated mice; $^{\#}P$<0.05, $^{\#\#}P$<0.01, $^{\#\#\#}P$<0.001, $^{\#\#\#\#}P$<0.0001 for mice in control versus SuHx groups; ns for no significance.

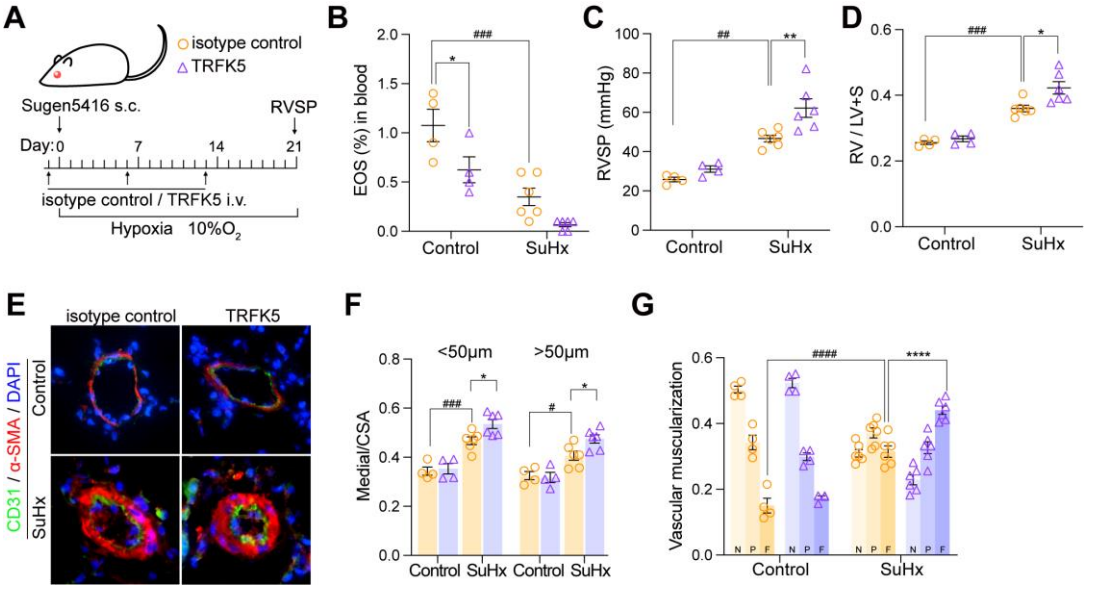

Supplementary Figure 7. EOS depletion exacerbated PH in rats.

A. Strategy for SuHx-induced PH in rats injected with isotype control antibody or TRFK5 (control: n=4 per group; SuHx: n=6 per group). **B.** The percentage of EOS among $CD45^{+}$ cells in peripheral blood of isotype control or TRFK5 treated rats. **C.** RVSP of isotype control or TRFK5 treated rats. **D.** RV/LV+S of the different experimental groups. **E.** Representative images of α-SMA and CD31 immunofluorescent staining of the lung sections from isotype control or TRFK5 treated rats. Scale bar=25 μm. **F.** Quantification of wall thickness of the pulmonary vasculature, for vessels of 20-50 μm and 50-100 μm in diameter, respectively. **G.** Proportion of non-muscularized (N), partially muscularized (P), or full muscularized (F) pulmonary vessels of 20-100 μm in diameter. All data are shown as mean ± SEM. Differences between multiple groups were evaluated by two-way ANOVA with Bonferroni's post hoc test. $^{*}P<0.05$, $^{**}P<0.01$ and $^{****}P<0.0001$ for TRFK5 versus isotype control-treated rats; $^{\#}P<0.05$, $^{\#\#}P<0.01$, $^{\#\#\#}P<0.001$ and $^{\#\#\#\#}P<0.0001$ for rats in control versus SuHx groups; ns for no significance.

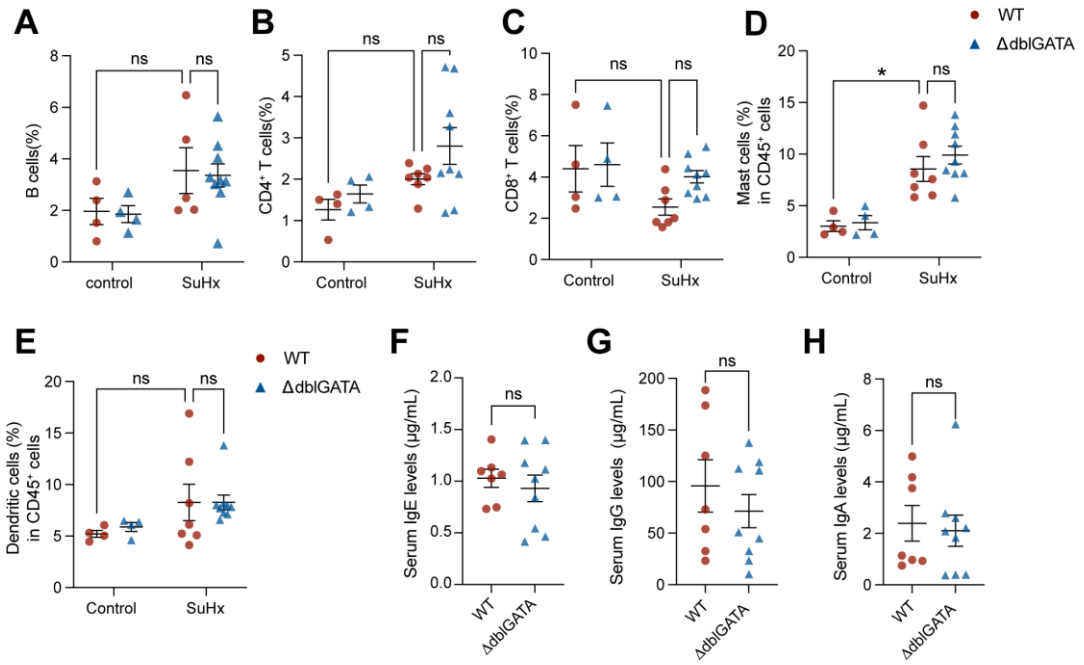

Supplementary Figure 8. Immune cell infiltration in lung of WT or ΔdblGATA mice.

A. The percentage of $CD19^+$ B cells in lung tissues of WT or ΔdblGATA mice (control: n=4 per group; PH: WT, n=5, ΔdblGATA, n=8). **B.** The percentage of $CD3^+CD4^+$ T cells among $CD45^+$ cells in lung tissues of WT or ΔdblGATA mice. **C.** The percentage of $CD3^+CD8^+$ T cells among $CD45^+$ cells in lung tissues of WT or ΔdblGATA mice. **D.** The percentage of $CD45^+Fc\varepsilon RI\alpha^+C\text{-}kit^+$ mast cells among $CD45^+$ cells in lung tissues of WT or ΔdblGATA mice. **E.** The percentage of $CD45^+CD11c^+MHCII^+$ dendritic cells among $CD45^+$ cells in lung tissues of WT or ΔdblGATA mice. **F.** Lung IgE levels of WT or ΔdblGATA mice with PH. **G.** Lung IgG levels of WT or ΔdblGATA mice with PH. **H.** Lung IgA levels of WT or ΔdblGATA mice with PH. For B-E, control: n=4 per group; SuHx: n=7 for WT, n=9 for ΔdblGATA. For F-H, n=7 for WT, n=9 for ΔdblGATA. All data are shown as mean ± SEM. For A-E, differences between multiple groups were evaluated by two-way ANOVA with Bonferroni's post hoc test. For F-H, differences between groups were evaluated by unpaired two-tailed Student's *t* test. **P*<0.05; ns for no significance.

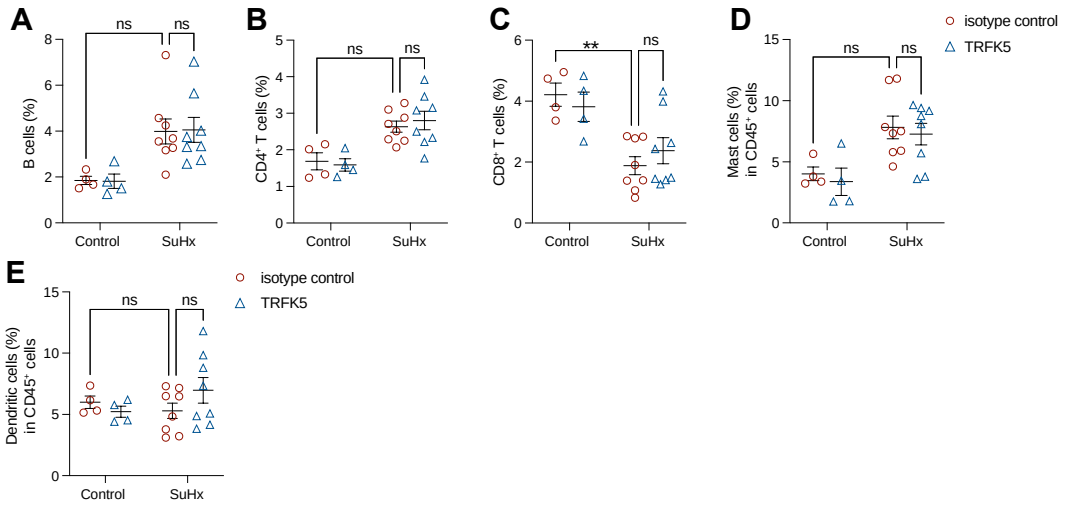

Supplementary Figure 9. Immune cells infiltration in lung of mice treated with isotype control or TRFK5.

A. The percentage of $CD19^+$ B cells in lung tissues of mice treated with isotype control or TRFK5. **B.** The percentage of $CD3^+CD4^+$ T cells in lung tissues of mice treated with isotype control or TRFK5. **C.** The percentage of $CD3^+CD8^+$ T cells among $CD45^+$ cells in lung tissues of mice treated with isotype control or TRFK5. **D.** The percentage of $CD45^+Fc\varepsilon RI\alpha^+C\text{-}kit^+$ mast cells among $CD45^+$ cells in lung tissues of mice treated with isotype control or TRFK5. **E.** The percentage of among $CD45^+$ cells $CD45^+CD11c^+MHCII^+$ dendritic cells in lung tissues of mice treated with isotype control or TRFK5. For A-E, control: n=4 per group; SuHx: n=8 per group. All data are shown as mean ± SEM. Differences between multiple groups were evaluated by two-way ANOVA with Bonferroni's post hoc test. $^{**}P<0.01$; ns for no significance.

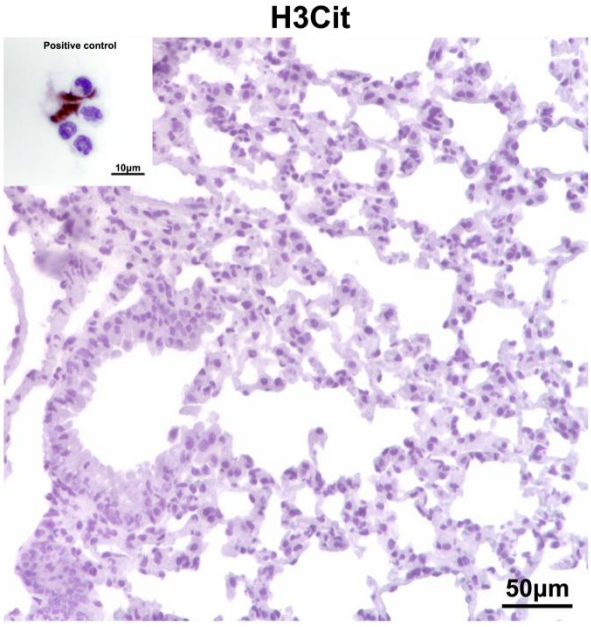

Supplementary Figure 10. H3cit immunohistochemical staining in lungs of PH mice.

Representative images of Histone H3Cit immunohistochemical staining of lung sections from PH mice and positive control from bronchoalveolar lavage fluid of pneumoconiosis mice. Scale bar=50 μm and 10 μm.

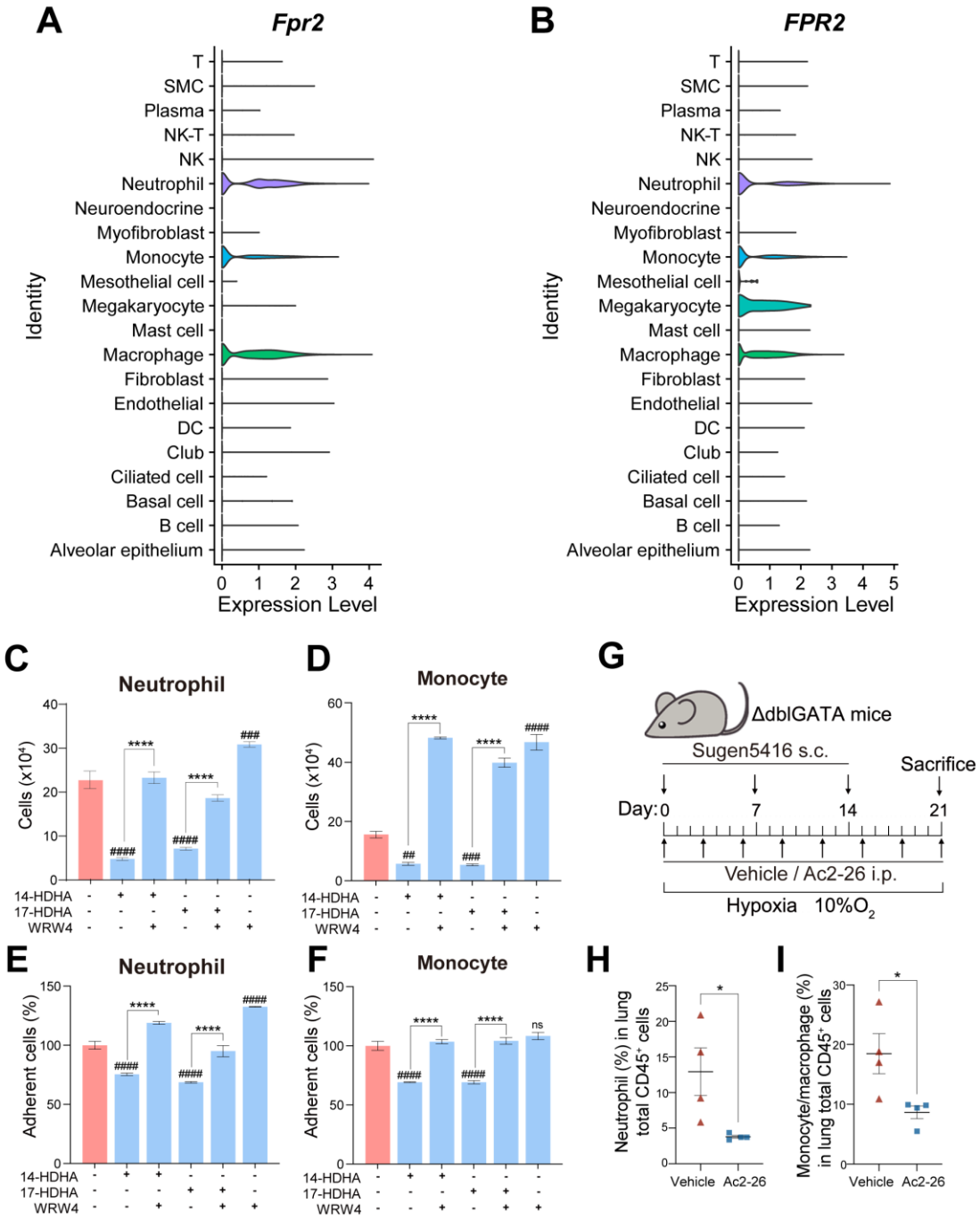

Supplementary Figure 11. 14/17-HDHA-FPR2 axis prevents neutrophil and monocyte/macrophage infiltration.

A. Violin plots of the expression of *Fpr2* among cell clusters in mouse. **B.** Violin plots of the expression of *FPR2* among cell clusters in human. **C.** Numbers of neutrophils pre-incubated with 14/17-HDHA and WRW4 crossing transwell inserts in response to CXCL1. **D.** Numbers of monocytes pre-incubated with 14/17-HDHA and WRW4 crossing transwell inserts in response to CCL2. **E.** Adhesion of neutrophils pre-incubated with 14/17-HDHA and WRW4 to plates coated with ICAM-1-Fc. **F.**

Adhesion of monocytes pre-incubated with 14/17-HDHA and WRW4 to plates coated with ICAM-1–Fc. **G.** Strategy for SuHx-induced PH in mice injected with vehicle or AC2-26 (n=4 per group). **H.** The percentage of neutrophils among $CD45^+$ cells. **I.** The percentage of monocytes/macrophages among $CD45^+$ cells. All data are shown as mean ± SEM. For C-F, differences were evaluated by one-way ANOVA with Bonferroni's post hoc test. For H and I, differences were evaluated by unpaired two-tailed *t*-test. For C-F, $^{\#\#}P<0.01$, $^{\#\#\#}P<0.001$ and $^{\#\#\#\#}P<0.0001$ for treated group compared with untreated-control group, $^{*}P<0.05$ and $^{****}P<0.0001$ for other groups; ns for no significance. For H and I, $^{*}P<0.05$.

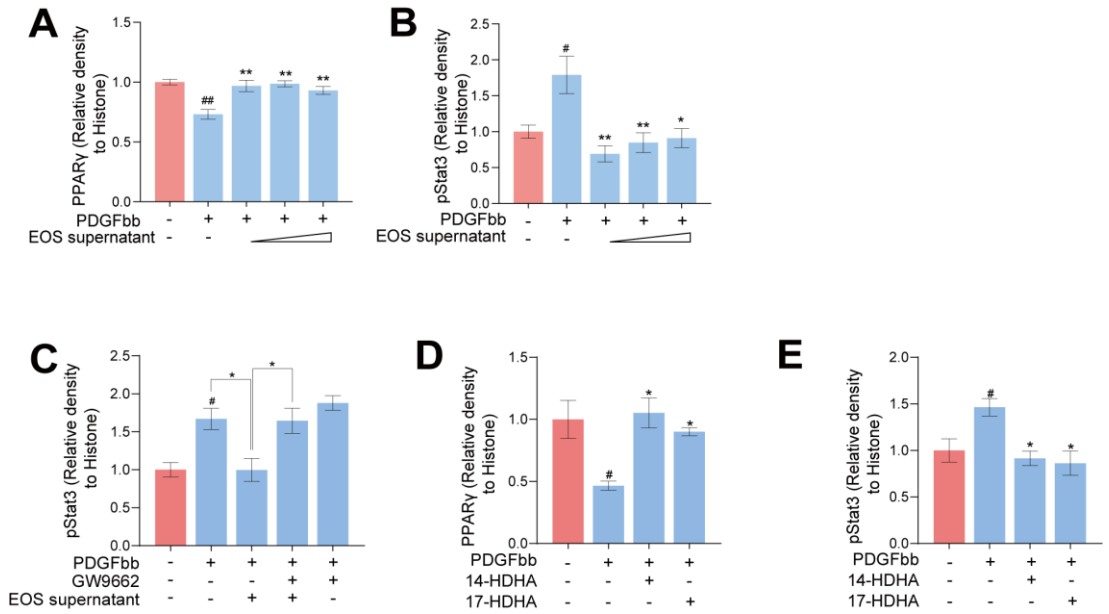

Supplementary Figure 12. Quantification of PPARγ and pStat3 in PASMCs

A. Quantification of PPARγ in cytoplasmic and nuclear extracts of mouse PASMC treated with PDGFbb and different concentrations of EOS supernatant (equivalent to 1×10^4, 1×10^5, 1×10^6 EOS per mL) for 24 h (n=3). **B.** Quantification of Stat3 and pStat3 in cytoplasmic and nuclear extracts of mouse PASMC treated with PDGFbb and different concentrations of EOS supernatant (equivalent to 1×10^4, 1×10^5, 1×10^6 EOS per mL) for 24 h (n=3). **C.** Quantification of Stat3 and pStat3 in cytoplasmic and nuclear extracts of mouse PASMC pre-incubated with GW9662 (1 μM) or DMSO for 24 h, then treated with PDGFbb and EOS supernatant (equivalent to 1×10^5 EOS per mL) for another 24 h (n=3). **D.** Quantification of PPARγ in cytoplasmic and nuclear extracts of mouse PASMC treated with PDGFbb and 14-HDHA, 17-HDHA (10 nM) for 24 h (n=3). **E.** Quantification of Stat3 and pStat3 in cytoplasmic and nuclear extracts of mouse PASMC treated with PDGFbb (10 ng/mL) and 14-HDHA, 17-HDHA (10 nM) for 24 h (n=3). All data are shown as mean ± SEM. Differences were evaluated by one-way ANOVA with Bonferroni's post hoc test. $^{\#}P<0.05$ and $^{\#\#}P<0.01$ for PDGFbb-treated group compared with untreated-control group; for C, $*P<0.05$ for other groups vs. EOS supernatant-treated group, for other panels, $*P<0.05$, $**P<0.01$ for other groups vs. PDGFbb-treated groups.

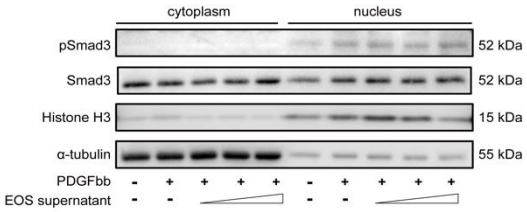

Supplementary Figure 13. Smad3 phosphorylation in PDGFbb-treated PASMCs with or without EOS supernatants.

Representative western blots of Smad3 and pSmad3 in cytoplasmic and nuclear extracts of mouse PASMC treated with PDGFbb and different concentrations of EOS supernatants (equivalent to 1×10^4, 1×10^5, 1×10^6 EOS per mL) for 24 h.

References

1. Wang L, Liu J, Wang W, Qi X, Wang Y, Tian B, Dai H, Wang J, Ning W, Yang T, Wang C. Targeting IL-17 attenuates hypoxia-induced pulmonary hypertension through downregulation of beta-catenin. *Thorax* 2019: 74(6): 564-578.
2. Kim K, Shim D, Lee JS, Zaitsev K, Williams JW, Kim KW, Jang MY, Seok Jang H, Yun TJ, Lee SH, Yoon WK, Prat A, Seidah NG, Choi J, Lee SP, Yoon SH, Nam JW, Seong JK, Oh GT, Randolph GJ, Artyomov MN, Cheong C, Choi JH. Transcriptome Analysis Reveals Nonfoamy Rather Than Foamy Plaque Macrophages Are Proinflammatory in Atherosclerotic Murine Models. *Circ Res* 2018: 123(10): 1127-1142.
3. Gallagher MP, Shrestha A, Magee JM, Wesemann DR. Detection of true IgE-expressing mouse B lineage cells. *J Vis Exp* 2014(94).
4. Tu L, Desroches-Castan A, Mallet C, Guyon L, Cumont A, Phan C, Robert F, Thuillet R, Bordenave J, Sekine A, Huertas A, Ritvos O, Savale L, Feige JJ, Humbert M, Bailly S, Guignabert C. Selective BMP-9 Inhibition Partially Protects Against Experimental Pulmonary Hypertension. *Circ Res* 2019: 124(6): 846-855.
5. Kikuchi N, Satoh K, Kurosawa R, Yaoita N, Elias-Al-Mamun M, Siddique MAH, Omura J, Satoh T, Nogi M, Sunamura S, Miyata S, Saito Y, Hoshikawa Y, Okada Y, Shimokawa H. Selenoprotein P Promotes the Development of Pulmonary Arterial Hypertension: Possible Novel Therapeutic Target. *Circulation* 2018: 138(6): 600-623.
6. Zheng GX, Terry JM, Belgrader P, Ryvkin P, Bent ZW, Wilson R, Ziraldo SB, Wheeler TD, McDermott GP, Zhu J, Gregory MT, Shuga J, Montesclaros L, Underwood JG, Masquelier DA, Nishimura SY, Schnall-Levin M, Wyatt PW, Hindson CM, Bharadwaj R, Wong A, Ness KD, Beppu LW, Deeg HJ, McFarland C, Loeb KR, Valente WJ, Ericson NG, Stevens EA, Radich JP, Mikkelsen TS, Hindson BJ, Bielas JH. Massively parallel digital transcriptional profiling of single cells. *Nat Commun* 2017: 8: 14049.
7. Butler A, Hoffman P, Smibert P, Papalexi E, Satija R. Integrating single-cell transcriptomic data across different conditions, technologies, and species. *Nat Biotechnol* 2018: 36(5): 411-420.
8. Satija R, Farrell JA, Gennert D, Schier AF, Regev A. Spatial reconstruction of single-cell gene expression data. *Nat Biotechnol* 2015: 33(5): 495-502.

9. Travaglini KJ, Nabhan AN, Penland L, Sinha R, Gillich A, Sit RV, Chang S, Conley SD, Mori Y, Seita J, Berry GJ, Shrager JB, Metzger RJ, Kuo CS, Neff N, Weissman IL, Quake SR, Krasnow MA. A molecular cell atlas of the human lung from single-cell RNA sequencing. *Nature* 2020: 587(7835): 619-625.
10. Dyer KD, Moser JM, Czapiga M, Siegel SJ, Percopo CM, Rosenberg HF. Functionally competent eosinophils differentiated ex vivo in high purity from normal mouse bone marrow. *J Immunol* 2008: 181(6): 4004-4009.
11. Cao Y, Zhang X, Wang L, Yang Q, Ma Q, Xu J, Wang J, Kovacs L, Ayon RJ, Liu Z, Zhang M, Zhou Y, Zeng X, Xu Y, Wang Y, Fulton DJ, Weintraub NL, Lucas R, Dong Z, Yuan JX, Sullivan JC, Meadows L, Barman SA, Wu C, Quan J, Hong M, Su Y, Huo Y. PFKFB3-mediated endothelial glycolysis promotes pulmonary hypertension. *Proc Natl Acad Sci U S A* 2019: 116(27): 13394-13403.